Journal of Sound and Vibration 329 (2010) 1101–1125

Contents lists available at ScienceDirect

Journal of Sound and Vibration

journal homepage: www.elsevier.com/locate/jsvi

Modelling of continuous and discontinuous floating slab tracks in a tunnel using a periodic approach

S. Gupta, G. Degrande *

Department of Civil Engineering, K.U.Leuven, Kasteelpark Arenberg 40, B-3001 Leuven, Belgium

ARTICLE INFO

Article history:
Received 23 December 2008
Received in revised form
27 October 2009
Accepted 29 October 2009
Handling Editor: M.P. Cartmell
Available online 1 December 2009

ABSTRACT

This paper presents a periodic approach to couple a track and a tunnel–soil system of different periodicity. The periodicity of the track and the tunnel–soil system is exploited using the Floquet transform to efficiently formulate the problem in the frequency–wavenumber domain as well as to limit the discretization effort to a reference cell. The track and the tunnel–soil system are modelled as two separate systems of different periodicity and are coupled in the frequency–wavenumber domain. A coupled periodic finite element–boundary element method is used to model the tunnel–soil system, while a periodic finite element model or an analytical approach is used to model the track.

A general analytical formulation to compute the response of three-dimensional periodic media that are excited by moving loads is discussed. It is shown that the response due to moving loads on the track can be calculated from the transfer function of the track–tunnel–soil system and the axle loads.

A methodology for computing the transfer functions of the coupled track–tunnel–soil system as well as the computation of dynamic forces accounting for the interaction between the moving vehicle and the periodic track are described. The model accounts for quasi-static forces as well as dynamic forces due to parametric excitation and unevenness excitation.

The methodology has been used to assess the vibration isolation efficiency of continuous and discontinuous floating slab tracks. It is concluded that both continuous and discontinuous floating slab tracks have a similar efficiency in the frequency range well above the isolation frequency of the slabs, which is usually higher than the slab passage frequency. In case of discontinuous slab tracks, the parametric excitation is found to be important, which results in a poorer performance of the track at low frequencies.

1. Introduction

Ground-borne vibrations induced by underground railways are a major environmental concern in urban areas. These vibrations propagate through the tunnel and the surrounding soil into nearby buildings, causing annoyance to people. Vibrations are perceived directly or they are sensed indirectly as re-radiated noise. The frequency range of interest for subway induced vibrations is 1–80 Hz and for re-radiated noise it is 16–250 Hz [1].

* Corresponding author.
E-mail addresses: shas.gupta@gmail.com (S. Gupta), geert.degrande@bwk.kuleuven.be (G. Degrande).

0022-460X/$ - see front matter © 2009 Elsevier Ltd. All rights reserved.
doi:10.1016/j.jsv.2009.10.037

To quantify these vibrations, great efforts have been made in recent years to develop prediction models. Yang et al. [2] have reviewed studies on ground-borne vibrations with emphasis on those induced by underground railways. Numerical models with varying degree of sophistication have been developed. Two-dimensional and three-dimensional numerical models based on the finite element method [3–6] or the coupled finite element–boundary element method [7,8] have been employed to model ground-borne vibration from railways. The two-dimensional models are not suitable for predicting subway induced vibrations as they do not account for wave propagation in the direction of the track and underestimate radiation damping into the soil. Three-dimensional models on the other hand, become computational very expensive for the application in the wide frequency range under consideration.

To overcome the shortcomings of two-dimensional and three-dimensional models, two-and-a-half dimensional and periodic models are often preferred. These models solve the three-dimensional dynamic track–tunnel–soil interaction in an efficient way, assuming that the geometry in the longitudinal direction is invariant or periodic. Two-and-a-half dimensional coupled finite element–boundary element models have the advantage that the discretization is only required over the cross section which can be of arbitrary geometry. The wave propagation in the longitudinal direction is represented in terms of discrete wavenumbers by application of a Fourier transform. Sheng et al. [9] and Anderson et al. [10] have used this approach to model vibrations from tunnels embedded in layered soils.

Researchers have also used alternative methods to model the soil around the tunnel. Bian et al. [11] have used a two-and-a-half dimensional finite element method with absorbing boundary conditions to model wave propagation from subway traffic. A two-and-a-half dimensional finite/infinite element approach to model ground-borne vibrations has been proposed by Yang et al. [12,13]. This model makes use of infinite elements at the boundaries of the finite element discretization of the soil domain and prevents the reflection of outgoing waves from the boundaries. Grundmann et al. [14] and Müller et al. [15] have proposed a two-and-a-half dimensional method based on a coupling of an integral transformation method and the finite element method (ITM–FEM). They model a ''generalized structure'' comprising the tunnel and a portion of the surrounding soil using the finite element method. The portion of the soil around the tunnel is chosen such that the complimentary domain is a half space with a cylindrical cavity, for which an analytical solution is obtained using the Integral Transform Method. The advantage of the approach is that it can account for an arbitrary geometry of the tunnel.

Within the framework of the CONVURT project, two modular numerical models have been developed to predict vibrations from excitation due to metro trains in tunnels for both newly built and existing situations: a pipe-in-pipe model [16–18] and a coupled periodic FE–BE model [19,20]. Both models account for the three-dimensional dynamic interaction between the track, the tunnel and the soil.

The pipe-in-pipe model assumes the geometry in the longitudinal direction to be invariant and uses the Fourier transform to formulate the problem in the frequency–wavenumber domain. The model is based on an analytical solution of the shell equations for the tunnel and the wave equations for an elastic continuum representing the soil [16,17].

The coupled periodic FE–BE model accounts for the complex periodic geometry of the tunnel as well as the layering of a semi-infinite soil medium. The periodic approach has been utilized for the seismic analysis of sheet pile walls of infinite length [21–23] and for dynamic analysis of tunnels embedded in a layered half-space [19,20].

The present paper concentrates on further developments of the coupled periodic finite element–boundary element model. The core of the model considering the dynamic tunnel–soil interaction problem has been presented by Clouteau et al. [19] and Degrande et al. [20]. The periodicity of the tunnel and the soil in the longitudinal y-direction is exploited using the Floquet transform, limiting the discretization effort to a single bounded reference cell and formulating the problem in the frequency–wavenumber domain [19,20]. A subdomain formulation based on the finite element method for the tunnel and the boundary element method for the soil is used to solve the problem on the reference cell. The response of three-dimensional invariant or periodic media that are excited by moving loads is given by Chebli et al. [24] and applied by Gupta et al. [25] to predict vibrations on the Beijing metro network.

The track is coupled to the model using the Craig–Bampton substructuring technique [20,26]. The advantage of this approach is that the expensive calculation of the dynamic tunnel–soil interaction does not have to be repeated when an alternative track structure is introduced in the tunnel. To preserve the versatility of the approach, it has been assumed that the track and tunnel–soil system have the same periodicity and, therefore, the stiffness and mass properties of the track are smeared in the longitudinal direction [20,27].

The periodicity of the system can be disregarded if its influence on the transfer functions and the wheel–track interaction forces is negligible. The periodicity of the track usually arises due to discretely supported rails on sleepers or due to the presence of discontinuous slabs. The periodicity of the track importantly influences the transfer functions and the wheel–track interaction forces.

The geometry of the tunnel depends on the construction method. Segmented tunnels are periodic and are formed when a tunnel boring machine is employed for the construction. The tunnel periodicity may also arise due to stiffening of the tunnel lining at regular intervals. The influence of tunnel properties on the wheel–track interaction forces is small, as the stiffness of the tunnel invert is usually much higher than the stiffness of the track. The influence of the tunnel periodicity on the transfer function depends on the spatial period. For typical tunnel structures, the periodicity does not affect the transfer functions in the frequency range of interest between 1 and 80 Hz. In most cases, the tunnel can be modelled as an equivalent invariant structure.

The coupled periodic finite element–boundary element model also considers the invariant tunnel as a periodic structure. In this case, the length L of the reference cell can be arbitrarily chosen. The spatial period L has an influence on the size of the boundary element and finite element mesh as well as on the computation of the Green–Floquet functions. Hence, the size of the cell should be chosen judiciously. For periodic tracks where rails are discretely supported on sleepers, the spatial period of the track–tunnel–soil system can be chosen as equal to the distance between the sleepers, which is typically 0.6 m.

For the case of discontinuous floating slab tracks, the spatial period can be much larger. Slabs of length 3, 6 or even 12 m are commonly used on railway networks. In this case, it is not desirable to choose the period of the tunnel according to the track periodicity, as it may result in a reference cell with large number of degrees of freedom, which will substantially increase the computational cost. Moreover, if Craig–Bampton substructuring is used to incorporate the track in the tunnel [20,25,27], an alternative track structure would necessitate reconsidering the dynamic tunnel–soil interaction problem as the periodicity of the system changes. To overcome these shortcomings, an alternative approach is used to couple the track and the tunnel–soil system.

This paper addresses the situation where the track and the tunnel–soil system have different periodicity. Instead of formulating the problem on a common spatial period of the track–tunnel–soil system, an alternative scheme for the coupling of the track and the tunnel–soil system is presented and the dynamic response of a system with two spatial periods is analyzed. Metrikine et al. [28] have previously studied the dynamic response of a two-level catenary subjected to a moving load. This method is applicable to a large class of double periodic systems. In the present paper, an alternative procedure based on the Floquet transform is presented.

The numerical model is capable of dealing with various types of excitation mechanisms. A distinction can be made between the quasi-static and dynamic excitations. The most common excitation mechanisms that induce dynamic forces are random excitation due to rail and wheel unevenness, impact excitation due to rail joints, switches and wheel flats and parametric excitation. In the present paper, the quasi-static excitation and the dynamic excitation due to rail and wheel unevenness and spatial periodicity are investigated. Lombaert et al. [29,30] have proposed a methodology of coupling a moving vehicle to a track that is invariant in the longitudinal direction. In the present paper, dynamic vehicle–track interaction for a periodic track structure is elaborated. The approach of coupling a moving vehicle to the periodic track is inspired by the work of Nordborg [31,32]. Recently, Sheng et al. [33] have used a similar idea and presented a Fourier series approach to study interactions between moving wheels and a periodically supported rail.

To demonstrate the applicability of the approach, the vibration isolation efficiency of continuous and discontinuous floating slab tracks (FST) is compared. Hussein et al. [34], Lombaert et al. [35] and Gupta et al. [27] have previously studied the dynamic behavior of floating slab tracks. Hussein et al. [36,37] have modelled discontinuous slab tracks and studied the effect of slab discontinuity by computing the response to moving harmonic loads. In the present paper, the response to moving trains is computed by considering dynamic train–track–tunnel–soil interaction.

The paper is structured as follows. In Section 2, the definition of the Floquet transform and its properties are recalled. In Section 3, the response of periodic domains subjected to moving loads is discussed. In Section 4, the calculation of the transfer function of the track–tunnel–soil system accounting for different periodicity of the track and the tunnel–soil system is explained. Section 5 outlines the computation of the axle loads from the unevenness excitation for invariant and periodic geometries. Section 6 presents an application of the method, where free field vibrations due to a train running on a slab track, a continuous floating slab track and a discontinuous floating slab track are predicted. The isolation efficiency of the continuous and discontinuous floating slab tracks is compared.

2. Periodic approach

The periodic approach allows one to study a complex structure with a periodic geometry with a moderate computation effort. The approach is based on reducing the problem to a single bounded reference cell or a generic cell by application of the Floquet transformation. Clouteau et al. [19,21,22] have previously utilized this approach to study the dynamic behavior of very long structures such as diaphragm walls, quay walls and tunnels.

The Floquet transform has been widely used in studying the properties of crystals and lattices in solid state physics. The transformation is used to solve partial differential equations with periodic coefficients. The same methodology has been used to solve the Navier equations in the soil and tunnel domain, that are periodic in the longitudinal direction [19,21].

If the geometry is periodic, the position vector $\mathbf{x}$ of any point in the problem domain Ω is decomposed as $\mathbf{x}=\tilde{\mathbf{x}}+nL\mathbf{e}_y$, where $\tilde{\mathbf{x}}=\{x,\tilde{y},z\}^{\mathrm{T}}$ is the position vector in the generic cell $\tilde{\Omega}$ and n is the cell number (Fig. 1). The Floquet transformation $\tilde{f}(\tilde{\mathbf{x}},\kappa_y,\omega)$ of a non-periodic function $\hat{f}(\mathbf{x},\omega)=\hat{f}(\tilde{\mathbf{x}}+nL\mathbf{e}_y,\omega)$ defined on a three-dimensional domain Ω, that is periodic in the direction $\mathbf{e}_y$ with period L, transforms the distance nL between the n-th cell and the generic cell $\tilde{\Omega}$ to the wavenumber κ_y and is defined as [19,21]

$$\tilde{f}(\tilde{\mathbf{x}},\kappa_y,\omega)=\sum_{n=-\infty}^{+\infty}\hat{f}(\tilde{\mathbf{x}}+nL\mathbf{e}_y,\omega)\exp(+\mathrm{i}nL\kappa_y) \tag{1}$$

The wavenumber κ_y lies in $]-\pi/L,\pi/L[$, which is called the first propagation zone or Brillouin zone [38]. The complex valued function $\tilde{f}(\tilde{\mathbf{x}},\kappa_y,\omega)$ is a periodic function of the first kind of κ_y with a period $2\pi/L$, as the following periodicity

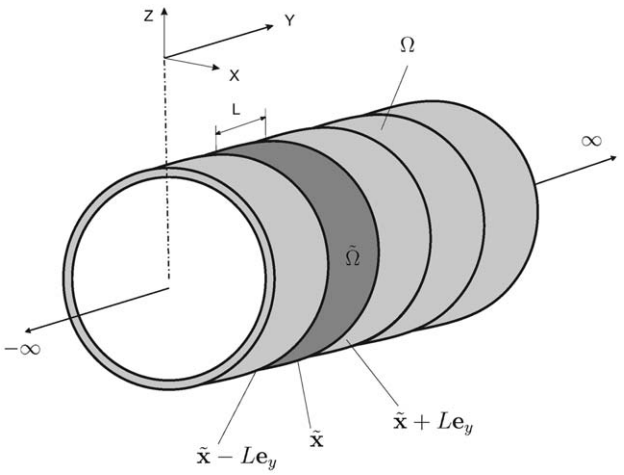

Fig. 1. Notations for periodic domains.

condition holds:

$$\tilde{f}\left(\tilde{\mathbf{x}}, \kappa_y + \frac{2\pi}{L}, \omega\right) = \tilde{f}(\tilde{\mathbf{x}}, \kappa_y, \omega) \tag{2}$$

This complex function $\tilde{f}(\tilde{\mathbf{x}}, \kappa_y, \omega)$ is also a periodic function of the second kind with a period L in the direction $\mathbf{e}_y$ since the following condition holds for all $\tilde{\mathbf{x}}$:

$$\tilde{f}(\tilde{\mathbf{x}} + L\mathbf{e}_y, \kappa_y, \omega) = \exp(-\mathrm{i}\kappa_y L)\tilde{f}(\tilde{\mathbf{x}}, \kappa_y, \omega) \tag{3}$$

It turns out that the Floquet transform commutes with differential operators with periodic coefficients. This allows for the restriction of the problem to periodic fields of the second kind defined on a generic cell $\tilde{\Omega}$. The function $f(\tilde{\mathbf{x}} + nL\mathbf{e}_y)$ can be reconstructed for any $\mathbf{x} = \tilde{\mathbf{x}} + nL\mathbf{e}_y$ using the inverse Floquet transform [19,21]:

$$f(\tilde{\mathbf{x}} + nL\mathbf{e}_y) = \frac{L}{2\pi}\int_{-\pi/L}^{+\pi/L} \tilde{f}(\tilde{\mathbf{x}}, \kappa_y, \omega)\exp(-\mathrm{i}nL\kappa_y)\,\mathrm{d}\kappa_y \tag{4}$$

3. Response to moving loads

The coupled track–tunnel–soil system is subjected to vertical loads moving along the longitudinal direction y. In the fixed frame of reference, the distribution of n_a vertical axle loads on the coupled track–tunnel–soil system is written as the summation of the product of Dirac functions that determine the time-dependent position $\mathbf{x}_k(t) = \{x_{k0}, y_{k0} + vt, z_{k0}\}^{\mathrm{T}}$ and the time history $g_k(t)$ of the k-th axle load:

$$\rho\mathbf{b}(\mathbf{x}, t) = \sum_{k=1}^{n_a} \delta(x - x_{k0})\delta(y - y_{k0} - vt)\delta(z - z_{k0})g_k(t)\mathbf{e}_z \tag{5}$$

y_{k0} is the initial position of the k-th axle that moves with the train speed v along the y-axis and $\mathbf{e}_z$ denotes the vertical unit vector.

A Fourier transformation is applied to Eq. (5) to obtain the representation in the frequency–spatial domain:

$$\rho\hat{b}_j(\mathbf{x}, \omega) = \frac{1}{v}\sum_{k=1}^{n_a} g_k\left(\frac{y - y_{k0}}{v}\right)\left[\exp\left(-\mathrm{i}\frac{\omega}{v}(y - y_{k0})\right)\right]\delta(x - x_{k0})\delta(z - z_{k0})\delta_{zj} \tag{6}$$

where $\rho\hat{b}_j(\mathbf{x}, \omega)$ is the frequency domain representation of the axle loads in index notation.

The response in the frequency domain $\hat{u}_i(\mathbf{x}, \omega)$ at the receiver point $\mathbf{x}$ due to n_a axle loads is written as the superposition of the load distribution along the source line:

$$\hat{u}_i(\mathbf{x}, \omega) = \int_{-\infty}^{\infty} \rho\hat{b}_j(\mathbf{x}', \omega)\hat{h}_{ji}(\mathbf{x}', \mathbf{x}, \omega)\,\mathrm{d}\mathbf{x}' \tag{7}$$

where $\hat{h}_{ji}(\mathbf{x}', \mathbf{x}, \omega)$ is the transfer function, expressing the displacement at $\mathbf{x}$ in the $\mathbf{e}_i$ direction, due to a unit load applied at $\mathbf{x}'$ in the $\mathbf{e}_j$ direction. Substituting Eq. (6) in Eq. (7) and elaborating the dependency of the transfer function $\hat{h}_{ji}(\mathbf{x}', \mathbf{x}, \omega)$ on

the source coordinates gives

$$\hat{u}_i(x,y,z,\omega)=\int_{-\infty}^{+\infty}\int_{-\infty}^{+\infty}\int_{-\infty}^{+\infty}\frac{1}{v}\sum_{k=1}^{n_a}\delta(x'-x_{k0})\delta(z'-z_{k0})g_k\left(\frac{y'-y_{k0}}{v}\right)\delta_{zj}\exp\left(-i\frac{\omega}{v}(y'-y_{k0})\right)\hat{h}_{ji}(x',y',z',x,y,z,\omega)\,dx'\,dy'\,dz'$$

$$=\frac{1}{v}\sum_{k=1}^{n_a}\int_{-\infty}^{\infty}g_k\left(\frac{y'-y_{k0}}{v}\right)\exp\left(-i\frac{\omega}{v}(y'-y_{k0})\right)\hat{h}_{zi}(x_{k0},y',z_{k0},x,y,z,\omega)\,dy' \tag{8}$$

Introducing a change of variables according to $\tau=(y'-y_{k0})/v$, this expression becomes:

$$\hat{u}_i(x,y,z,\omega)=\sum_{k=1}^{n_a}\int_{-\infty}^{\infty}g_k(\tau)\hat{h}_{zi}(x_{k0},y_{k0}+v\tau,z_{k0},x,y,z,\omega)\exp(-i\omega\tau)\,d\tau \tag{9}$$

The response due to a moving load can therefore be calculated from the time history $g_k(t)$ of the axle loads and the receptance $\hat{h}_{zi}(\mathbf{x}_k(t),\mathbf{x},\omega)$ of the track–tunnel–soil system describing the displacement at a point $\mathbf{x}$ in the direction $\mathbf{e}_i$ due to a unit impulse at the time-dependent position $\mathbf{x}_k(t)=\{x_{k0},y_{k0}+vt,z_{k0}\}^{\mathrm{T}}$ in the direction $\mathbf{e}_z$. In case of a periodic geometry, expressions (8) and (9) can be further simplified.

Chebli et al. [24] have outlined this approach and applied it for the case of moving harmonic loads on surface tracks. A periodic geometry has a spatial period L and it is assumed that the receiver point is in the generic cell $\mathbf{x}=\tilde{\mathbf{x}}$. In the following, only the dependence on the longitudinal y-coordinates is included. The axle load $g_k((y'-y_{k0})/v)$ in Eq. (8) is expressed in terms of its Fourier transform, so that the response becomes:

$$\hat{u}_i(\tilde{y},\omega)=\frac{1}{2\pi v}\sum_{k=1}^{n_a}\int_{-\infty}^{\infty}\int_{-\infty}^{\infty}\hat{g}_k(\tilde{\omega})\exp\left(-i\left(\frac{\omega-\tilde{\omega}}{v}\right)(y'-y_{k0})\right)d\tilde{\omega}\hat{h}_{zi}(y',\tilde{y},\omega)\,dy' \tag{10}$$

Splitting the integral with respect to y' to a summation and an integral over the cell and substituting $y'=\tilde{y}'+n'L$ gives

$$\hat{u}_i(\tilde{y},\omega)=\frac{1}{2\pi v}\sum_{k=1}^{n_a}\int_{-\infty}^{\infty}\hat{g}_k(\tilde{\omega})\int_{-L/2}^{L/2}\sum_{n'=-\infty}^{\infty}\exp\left(-i\left(\frac{\omega-\tilde{\omega}}{v}\right)(\tilde{y}'+n'L-y_{k0})\right)\hat{h}_{zi}(\tilde{y}'+n'L,\tilde{y},\omega)\,d\tilde{y}'\,d\tilde{\omega} \tag{11}$$

Due to the geometric periodicity, the following equation holds:

$$\hat{h}_{zi}(\tilde{y}'+n'L,\tilde{y},\omega)=\hat{h}_{zi}(\tilde{y}',\tilde{y}-n'L,\omega) \tag{12}$$

From Eqs. (11) and (12), the following expression is obtained:

$$\hat{u}_i(\tilde{y},\omega)=\frac{1}{2\pi v}\sum_{k=1}^{n_a}\int_{-\infty}^{\infty}\hat{g}_k(\tilde{\omega})\exp\left(i\left(\frac{\omega-\tilde{\omega}}{v}\right)y_{k0}\right)\int_{-L/2}^{L/2}\exp\left(-i\left(\frac{\omega-\tilde{\omega}}{v}\right)\tilde{y}'\right)$$
$$\times\left[\sum_{n'=-\infty}^{\infty}\exp\left(-i\left(\frac{\omega-\tilde{\omega}}{v}\right)(n'L)\right)\hat{h}_{zi}(\tilde{y}',\tilde{y}-n'L,\omega)\right]d\tilde{y}'\,d\tilde{\omega} \tag{13}$$

A change of variables according to $n'=-n$ is introduced in Eq. (13) to obtain

$$\hat{u}_i(\tilde{y},\omega)=\frac{1}{2\pi v}\sum_{k=1}^{n_a}\int_{-\infty}^{\infty}\hat{g}_k(\tilde{\omega})\exp\left(i\left(\frac{\omega-\tilde{\omega}}{v}\right)y_{k0}\right)\int_{-L/2}^{L/2}\exp\left(-i\left(\frac{\omega-\tilde{\omega}}{v}\right)\tilde{y}'\right)$$
$$\times\left[\sum_{n=-\infty}^{\infty}\exp\left(i\left(\frac{\omega-\tilde{\omega}}{v}\right)(nL)\right)\hat{h}_{zi}(\tilde{y}',\tilde{y}+nL,\omega)\right]d\tilde{y}'\,d\tilde{\omega} \tag{14}$$

Any value of $(\omega-\tilde{\omega})/v$ in the range $]-\infty,\infty[$ can be mapped to the wavenumber $\kappa_y\in]-\pi/L,\pi/L[$ using the relation $(\omega-\tilde{\omega})/v=\kappa_y+2m\pi/L$ with m an integer. Invoking this relationship in the bracketed terms of Eq. (14) gives

$$\hat{u}_i(\tilde{y},\omega)=\frac{1}{2\pi v}\sum_{k=1}^{n_a}\int_{-\infty}^{\infty}\hat{g}_k(\tilde{\omega})\exp\left(i\left(\frac{\omega-\tilde{\omega}}{v}\right)y_{k0}\right)\int_{-L/2}^{L/2}\exp\left(-i\left(\frac{\omega-\tilde{\omega}}{v}\right)\tilde{y}'\right)\left[\sum_{n=-\infty}^{\infty}\exp(i\kappa_y nL)\hat{h}_{zi}(\tilde{y}',\tilde{y}+nL,\omega)\right]d\tilde{y}'\,d\tilde{\omega} \tag{15}$$

The bracketed term is the Floquet transform $\tilde{h}_{zi}(\tilde{y}',\tilde{y},\kappa_y,\omega)$ of the transfer function $\hat{h}_{zi}(\tilde{y}',\tilde{y}+nL,\omega)$. Thus, expression (15) can be written in terms of the transfer function in the frequency–wavenumber domain:

$$\hat{u}_i(\tilde{y},\omega)=\frac{1}{2\pi v}\sum_{k=1}^{n_a}\int_{-\infty}^{\infty}\hat{g}_k(\tilde{\omega})\exp\left(i\left(\frac{\omega-\tilde{\omega}}{v}\right)y_{k0}\right)\int_{-L/2}^{L/2}\exp\left(-i\left(\frac{\omega-\tilde{\omega}}{v}\right)\tilde{y}'\right)\tilde{h}_{zi}(\tilde{y}',\tilde{y},\kappa_y,\omega)\,d\tilde{y}'\,d\tilde{\omega} \tag{16}$$

where $\kappa_y=(\omega-\tilde{\omega})/v-2m\pi/L$ and $\kappa_y\in]-\pi/L,\pi/L[$. The response at any other point $\mathbf{x}=\tilde{\mathbf{x}}+nL\mathbf{e}_y$ is given by

$$\hat{u}_i(\tilde{y}+nL,\omega)=\frac{1}{2\pi v}\sum_{k=1}^{n_a}\int_{-\infty}^{\infty}\hat{g}_k(\tilde{\omega})\exp\left(i\left(\frac{\omega-\tilde{\omega}}{v}\right)y_{k0}\right)\int_{-L/2}^{L/2}\exp\left(-i\left(\frac{\omega-\tilde{\omega}}{v}\right)\tilde{y}'\right)\tilde{h}_{zi}(\tilde{y}',\tilde{y}+nL,\kappa_y,\omega)\,d\tilde{y}'\,d\tilde{\omega} \tag{17}$$

Using the periodicity condition of the second kind (3) on the transfer function and invoking the relation $\kappa_y = (\omega - \tilde{\omega})/v - 2m\pi/L$ gives

$$\hat{u}_i(\tilde{y}+nL,\omega) = \frac{1}{2\pi v}\sum_{k=1}^{n_a}\int_{-\infty}^{\infty}\hat{g}_k(\tilde{\omega})\int_{-L/2}^{L/2}\exp\left(-\mathrm{i}\left(\frac{\omega-\tilde{\omega}}{v}\right)\tilde{y}'\right)\tilde{h}_{zi}(\tilde{y}',\tilde{y},\kappa_y,\omega)\,\mathrm{d}\tilde{y}'\exp\left(-\mathrm{i}\left(\frac{\omega-\tilde{\omega}}{v}\right)(nL-y_{k0})\right)\mathrm{d}\tilde{\omega} \quad (18)$$

A change of variables according to $k_y = (\omega - \tilde{\omega})/v$ yields:

$$\hat{u}_i(\tilde{y}+nL,\omega) = \frac{1}{2\pi}\sum_{k=1}^{n_a}\int_{-\infty}^{\infty}\hat{g}_k(\tilde{\omega})\int_{-L/2}^{L/2}\exp(-\mathrm{i}k_y\tilde{y}')\tilde{h}_{zi}(\tilde{y}',\tilde{y},\kappa_y,\omega)\,\mathrm{d}\tilde{y}'\exp(-\mathrm{i}k_y(nL-y_{k0}))\,\mathrm{d}k_y \quad (19)$$

where $\kappa_y = k_y - 2m\pi/L$.

The advantage of the present approach is that the response due to moving loads can be directly deduced from the transfer functions in the frequency–wavenumber domain. In the following, the computation of the transfer functions and the axle loads is explained.

4. Transfer functions

The transfer functions $\tilde{h}_{zi}(\tilde{y}',\tilde{y},\kappa_y,\omega)$ in Eq. (19) are computed by means of the coupled periodic finite element–boundary element model using the classical domain decomposition approach based on the finite element method for the track and the tunnel and the boundary element method for the soil [19–22].

Let the tunnel–soil system be modelled as a periodic structure with spatial period L_1, while the spatial period of the track is L_2. The Floquet transformation is applied to the tunnel–soil system and the track structure to restrict the problem domain Ω to the reference cells $\tilde{\Omega}_1$ and $\tilde{\Omega}_2$ of lengths L_1 and L_2, respectively. The problem is formulated on the respective reference cells in the frequency–wavenumber domain. The wavenumbers for the reference cells $\tilde{\Omega}_1$ and $\tilde{\Omega}_2$ are $\kappa_{y_1} \in]-\pi/L_1,\pi/L_1[$ and $\kappa_{y_2} \in]-\pi/L_2,\pi/L_2[$, respectively.

The track is coupled to the tunnel via springs that have a certain vertical stiffness and zero lateral stiffness. The coupling of the track and the tunnel is performed in the frequency–wavenumber domain on a reference cell of length L, which is equal to the lowest common multiple of L_1 and L_2.

To illustrate the procedure of coupling, the common spatial period $L = M_2L_2 = M_1L_1$ is considered, where M_1 and M_2 are positive integers. Let the reference cell corresponding to the common spatial period L be denoted by $\tilde{\Omega} = \tilde{\Omega}_{\mathrm{ts}} \cup \tilde{\Omega}_{t_{\mathrm{r}}}$ and the wavenumbers associated with it be $\kappa_y \in [-\pi/L,\pi/L]$. Here $\tilde{\Omega}_{\mathrm{ts}}$ and $\tilde{\Omega}_{t_{\mathrm{r}}}$ denote the reference cell of length L corresponding to the tunnel–soil system and the track system, respectively.

The dynamic tunnel–soil interaction problem is tackled using the coupled periodic finite element–boundary element model. The displacement field $\tilde{\mathbf{u}}_t(\tilde{\mathbf{x}}_1,\kappa_{y_1},\omega)$ in the tunnel is decomposed on a basis of functions $\tilde{\boldsymbol{\Psi}}_t(\tilde{\mathbf{x}}_1,\kappa_{y_1})$, which are periodic of the second kind:

$$\tilde{\mathbf{u}}_t(\tilde{\mathbf{x}}_1,\kappa_{y_1},\omega) = \tilde{\boldsymbol{\Psi}}_t(\tilde{\mathbf{x}}_1,\kappa_{y_1})\tilde{\boldsymbol{\alpha}}_t(\kappa_{y_1},\omega) \quad (20)$$

Likewise, the soil displacements $\tilde{\mathbf{u}}_s(\tilde{\mathbf{x}}_1,\kappa_{y_1},\omega)$ in the reference cell $\tilde{\Omega}_1$ are written as a superposition of waves that are radiated from the tunnel into the soil:

$$\tilde{\mathbf{u}}_s(\tilde{\mathbf{x}}_1,\kappa_{y_1},\omega) = \tilde{\mathbf{u}}_{\mathrm{sc}}(\tilde{\mathbf{u}}_t(\tilde{\mathbf{x}}_1,\kappa_{y_1},\omega)) = \sum_{m=1}^{M}\tilde{\mathbf{u}}_{\mathrm{sc}}(\tilde{\boldsymbol{\psi}}_{\mathrm{tm}}(\tilde{\mathbf{x}}_1,\kappa_{y_1},\omega))\tilde{\alpha}_{\mathrm{tm}}(\kappa_{y_1},\omega) \quad (21)$$

where $\tilde{\mathbf{u}}_{\mathrm{sc}}(\tilde{\mathbf{u}}_t)$ is the wave field scattered in the ground due to the displacements $\tilde{\mathbf{u}}_t$ of the tunnel. The decomposition of the displacement field $\tilde{\mathbf{u}}_t$ into the tunnel modes $\tilde{\boldsymbol{\psi}}_{\mathrm{tm}}$ is introduced in Eq. (21). The soil displacements $\tilde{\mathbf{u}}_s$ are then written as the superposition of the scattered wave field $\tilde{\mathbf{u}}_{\mathrm{sc}}(\tilde{\boldsymbol{\psi}}_{\mathrm{tm}})$ due to each tunnel mode $\tilde{\boldsymbol{\psi}}_{\mathrm{tm}}$.

The coupled system of equations in the frequency–wavenumber domain is given by [19–22]

$$[\tilde{\mathbf{K}}_t(\kappa_{y_1}) - \omega^2\tilde{\mathbf{M}}_t(\kappa_{y_1}) + \tilde{\mathbf{K}}_s(\kappa_{y_1},\omega)]\tilde{\boldsymbol{\alpha}}_t(\kappa_{y_1},\omega) = \tilde{\mathbf{F}}_t(\kappa_{y_1},\omega) \quad (22)$$

where $\tilde{\boldsymbol{\alpha}}_t(\kappa_{y_1},\omega)$ are the unknown modal coordinates. $\tilde{\mathbf{K}}_t(\kappa_{y_1}) - \omega^2\tilde{\mathbf{M}}_t(\kappa_{y_1})$ is the dynamic stiffness matrix of the tunnel in the frequency–wavenumber domain calculated using a finite element method. $\tilde{\mathbf{K}}_s(\kappa_{y_1},\omega)$ is the dynamic stiffness matrix of the soil calculated with a periodic boundary element formulation based on Green–Floquet functions defined on the periodic structure with period L_1 along the tunnel [19,21–23]. $\tilde{\mathbf{F}}_t(\kappa_{y_1},\omega)$ is the force vector defined on the reference cell $\tilde{\Omega}_1$.

The transfer functions $\tilde{\mathbf{H}}_{t_t}(\tilde{\mathbf{x}}_1',\tilde{\mathbf{x}}_1,\kappa_{y_1},\omega)$, which denote the displacement of the tunnel at $\tilde{\mathbf{x}}_1$ due to a unit load applied at $\tilde{\mathbf{x}}_1'$ can be calculated with help of Eqs. (22) and (20) for different positions of the load. The transfer function expressing the soil displacements is denoted as $\tilde{\mathbf{H}}_s(\tilde{\mathbf{x}}_1',\tilde{\mathbf{x}}_1,\kappa_{y_1},\omega)$ and can be calculated using Eq. (21).

Since the tunnel has been modelled with a periodicity L_1 different from the periodicity L_2 of the track, the transfer functions of the tunnel $\tilde{\mathbf{H}}_{t_t}(\tilde{\mathbf{x}}_1',\tilde{\mathbf{x}}_1,\kappa_{y_1},\omega)$ and the transfer function of the soil $\tilde{\mathbf{H}}_s(\tilde{\mathbf{x}}_1',\tilde{\mathbf{x}}_1,\kappa_{y_1},\omega)$ defined on the reference cell $\tilde{\Omega}_1$ have to be expressed on the reference cell $\tilde{\Omega}_{\mathrm{ts}}$ of length L. For the coupling of the track and tunnel–soil system, it is necessary to express the solution of both systems on the reference cell $\tilde{\Omega}$, which has a common spatial period L. The superscript t or s in the transfer function has been omitted to explain this procedure.

Since $L=M_1L_1$, any point $\tilde{\mathbf{x}}$ in the reference cell $\tilde{\Omega}$ can be mapped to a point $\tilde{\mathbf{x}}_1$ in the reference cell $\tilde{\Omega}_1$ using the relation $\tilde{\mathbf{x}}=\tilde{\mathbf{x}}_1+mL_1\mathbf{e}_y$, where m is a positive integer less than M_1. The displacement $\tilde{\mathbf{H}}(\tilde{\mathbf{x}}_1'+mL_1\mathbf{e}_y,\tilde{\mathbf{x}}_1,\kappa_{y_1},\omega)$ at $\tilde{\mathbf{x}}_1$ due to a load at $\tilde{\mathbf{x}}'=\tilde{\mathbf{x}}_1'+mL_1\mathbf{e}_y$ can be written using the periodicity condition of the second kind:

$$\tilde{\mathbf{H}}(\tilde{\mathbf{x}}_1'+mL_1\mathbf{e}_y,\tilde{\mathbf{x}}_1,\kappa_{y_1},\omega)=\tilde{\mathbf{H}}(\tilde{\mathbf{x}}_1',\tilde{\mathbf{x}}_1,\kappa_{y_1},\omega)\exp(\mathrm{i}m\kappa_{y_1}L_1) \tag{23}$$

To express the transfer functions on the reference cell $\tilde{\Omega}$, the relations between the Fourier and the Floquet transformation are exploited [24,39]. These relations have been derived in Appendix A. Let $\tilde{\hat{\mathbf{H}}}(\tilde{\mathbf{x}}',k_y,\omega)$ be the Fourier transform of the transfer function $\hat{\mathbf{H}}(\tilde{\mathbf{x}}',\mathbf{x},\omega)$ with respect to the receiver coordinate y. For the sake of brevity the dependence of the transfer functions on the receiver coordinates x and z is omitted.

First the Floquet transform $\tilde{\mathbf{H}}(\tilde{\mathbf{x}},\tilde{\mathbf{x}}_1,\kappa_{y_1},\omega)$ is used to find the Fourier transform $\tilde{\hat{\mathbf{H}}}(\tilde{\mathbf{x}}',k_y,\omega)$:

$$\tilde{\hat{\mathbf{H}}}(\tilde{\mathbf{x}}',k_y,\omega)=\int_{-L_1/2}^{L_1/2}\tilde{\mathbf{H}}(\tilde{\mathbf{x}}',\tilde{\mathbf{x}}_1,\kappa_{y_1},\omega)\exp(\mathrm{i}k_y\tilde{y}_1)\,\mathrm{d}\tilde{y}_1 \tag{24}$$

Subsequently, the Fourier transform $\tilde{\hat{\mathbf{H}}}(\tilde{\mathbf{x}}',k_y,\omega)$ is used to find the Floquet transform $\tilde{\mathbf{H}}(\tilde{\mathbf{x}}',\tilde{\mathbf{x}},\kappa_y,\omega)$ on a larger cell:

$$\tilde{\mathbf{H}}(\tilde{\mathbf{x}}',\tilde{\mathbf{x}},\kappa_y,\omega)=\frac{1}{L}\sum_{n=-\infty}^{\infty}\tilde{\hat{\mathbf{H}}}(\tilde{\mathbf{x}}',k_y,\omega)\exp[-\mathrm{i}(\kappa_y+n2\pi/L)\tilde{y}] \tag{25}$$

where $k_y=\kappa_{y_1}+n_12\pi/L_1=\kappa_y+n2\pi/L$.

It should be emphasized that the dynamic tunnel–soil interaction problem is solved in the frequency–wavenumber domain on a smaller reference cell $\tilde{\Omega}_1$ and the basic properties of the Floquet transformation are used to express the solution on a larger cell $\tilde{\Omega}_{\mathrm{ts}}$. This is vital for the coupling of the track and the tunnel–soil system.

The equilibrium equation can be written in terms of the transfer functions $\tilde{\mathbf{H}}_{t_t}(\tilde{\mathbf{x}}',\tilde{\mathbf{x}},\kappa_y,\omega)$ defined on the reference cell $\tilde{\Omega}_{\mathrm{ts}}$:

$$\begin{bmatrix}\tilde{\mathbf{H}}_{t_t}(\tilde{\mathbf{x}}_i',\tilde{\mathbf{x}}_i,\kappa_y,\omega) & \tilde{\mathbf{H}}_{t_t}(\tilde{\mathbf{x}}_c',\tilde{\mathbf{x}}_i,\kappa_y,\omega)\\ \tilde{\mathbf{H}}_{t_t}(\tilde{\mathbf{x}}_i',\tilde{\mathbf{x}}_c,\kappa_y,\omega) & \tilde{\mathbf{H}}_{t_t}(\tilde{\mathbf{x}}_c',\tilde{\mathbf{x}}_c,\kappa_y,\omega)\end{bmatrix}\begin{Bmatrix}\mathbf{0}\\ \tilde{\mathbf{P}}_{t_t}(\kappa_y,\omega)\end{Bmatrix}=\begin{Bmatrix}\tilde{\mathbf{u}}_{t_t}(\tilde{\mathbf{x}}_i,\kappa_y,\omega)\\ \tilde{\mathbf{u}}_{t_t}(\tilde{\mathbf{x}}_c,\kappa_y,\omega)\end{Bmatrix} \tag{26}$$

where the tunnel displacements $\tilde{\mathbf{u}}_{t_t}(\tilde{\mathbf{x}},\kappa_y,\omega)$ are separated into the displacement degrees of freedom of the tunnel coupled to the track $\tilde{\mathbf{u}}_{t_t}(\tilde{\mathbf{x}}_c,\kappa_y,\omega)$ and the remaining degrees of freedom of the tunnel $\tilde{\mathbf{u}}_{t_t}(\tilde{\mathbf{x}}_i,\kappa_y,\omega)$. $\tilde{\mathbf{P}}_{t_t}$ is the reaction force on the tunnel arising from the coupling of the track.

Likewise, the free field displacements $\tilde{\mathbf{u}}_s(\tilde{\mathbf{x}},\kappa_y,\omega)$ can be written in terms of the transfer function $\tilde{\mathbf{H}}_s(\tilde{\mathbf{x}}_c',\tilde{\mathbf{x}},\kappa_y,\omega)$:

$$\tilde{\mathbf{H}}_s(\tilde{\mathbf{x}}_c',\tilde{\mathbf{x}},\kappa_y,\omega)\tilde{\mathbf{P}}_{t_t}(\kappa_y,\omega)=\tilde{\mathbf{u}}_s(\tilde{\mathbf{x}},\kappa_y,\omega) \tag{27}$$

The displacements of the free track can be calculated in the frequency–wavenumber domain on the reference cell $\tilde{\Omega}_2$. The track can be modelled analytically or using the periodic FE approach. The transfer functions $\tilde{\mathbf{H}}_{t_r}(\tilde{\mathbf{x}}_2',\tilde{\mathbf{x}}_2,\kappa_{y_2},\omega)$ of the free track on the reference cell $\tilde{\Omega}_2$ are defined as the displacement at $\tilde{\mathbf{x}}_2$ due to a unit load applied at $\tilde{\mathbf{x}}_2'$. The transfer functions $\tilde{\mathbf{H}}_{t_r}(\tilde{\mathbf{x}}',\tilde{\mathbf{x}},\kappa_y,\omega)$ on the reference cell $\tilde{\Omega}_{t_r}$ of length L can be obtained using Eqs. (23)–(25). The equilibrium of the track can be written on the reference cell $\tilde{\Omega}_{t_r}$ as

$$\begin{bmatrix}\tilde{\mathbf{H}}_{t_r}(\tilde{\mathbf{x}}_i',\tilde{\mathbf{x}}_i,\kappa_y,\omega) & \tilde{\mathbf{H}}_{t_r}(\tilde{\mathbf{x}}_c',\tilde{\mathbf{x}}_i,\kappa_y,\omega)\\ \tilde{\mathbf{H}}_{t_r}(\tilde{\mathbf{x}}_i',\tilde{\mathbf{x}}_c,\kappa_y,\omega) & \tilde{\mathbf{H}}_{t_r}(\tilde{\mathbf{x}}_c',\tilde{\mathbf{x}}_c,\kappa_y,\omega)\end{bmatrix}\begin{Bmatrix}\tilde{\mathbf{f}}_{t_r}\\ -\tilde{\mathbf{P}}_{t_t}(\kappa_y,\omega)\end{Bmatrix}=\begin{Bmatrix}\tilde{\mathbf{u}}_{t_r}(\tilde{\mathbf{x}}_i,\kappa_y,\omega)\\ \tilde{\mathbf{u}}_{t_r}(\tilde{\mathbf{x}}_c,\kappa_y,\omega)\end{Bmatrix} \tag{28}$$

where subscripts c and i refers to the degrees of freedom of the track coupled to the tunnel and the remaining degrees of freedom of the track, respectively. $\tilde{\mathbf{f}}_{t_r}$ is the external load acting on the track.

The equilibrium equation of the springs that couple the track and the tunnel is given by

$$\mathbf{K}_{\mathrm{sb}}(\tilde{\mathbf{u}}_{t_r}(\tilde{\mathbf{x}}_c,\kappa_y,\omega)-\tilde{\mathbf{u}}_{t_t}(\tilde{\mathbf{x}}_c,\kappa_y,\omega))=\tilde{\mathbf{P}}_{t_t}(\kappa_y,\omega) \tag{29}$$

where $\mathbf{K}_{\mathrm{sb}}$ is the matrix characterizing the dynamic stiffness of the springs and $\tilde{\mathbf{u}}_{t_t}(\tilde{\mathbf{x}}_c,\kappa_y,\omega)$ and $\tilde{\mathbf{u}}_{t_r}(\tilde{\mathbf{x}}_c,\kappa_y,\omega)$ are the tunnel and the track displacements of the degrees of freedom that are coupled by spring elements.

Substituting Eqs. (26) and (28) in Eq. (29) results in

$$[\mathbf{K}_{\mathrm{sb}}\tilde{\mathbf{H}}_{t_r}(\tilde{\mathbf{x}}_c',\tilde{\mathbf{x}}_c,\kappa_y,\omega)+\mathbf{K}_{\mathrm{sb}}\tilde{\mathbf{H}}_{t_t}(\tilde{\mathbf{x}}_c',\tilde{\mathbf{x}}_c,\kappa_y,\omega)+\mathbf{I}]\tilde{\mathbf{P}}_{t_t}(\kappa_y,\omega)=\mathbf{K}_{\mathrm{sb}}\tilde{\mathbf{H}}_{t_r}(\tilde{\mathbf{x}}_i',\tilde{\mathbf{x}}_c,\kappa_y,\omega)\tilde{\mathbf{f}}_{t_r} \tag{30}$$

where $\mathbf{I}$ is an identity matrix of dimensions corresponding to the number of degrees of freedom of the track that are coupled to the tunnel. It must be noted that if the connection between the track and the tunnel is rigid, the relation between the reaction force and external force is reduced to the following:

$$[\tilde{\mathbf{H}}_{t_r}(\tilde{\mathbf{x}}_c',\tilde{\mathbf{x}}_c,\kappa_y,\omega)+\tilde{\mathbf{H}}_{t_t}(\tilde{\mathbf{x}}_c',\tilde{\mathbf{x}}_c,\kappa_y,\omega)]\tilde{\mathbf{P}}_{t_t}(\kappa_y,\omega)=\tilde{\mathbf{H}}_{t_r}(\tilde{\mathbf{x}}_i',\tilde{\mathbf{x}}_c,\kappa_y,\omega)\tilde{\mathbf{f}}_{t_r} \tag{31}$$

Alternatively, one could also work with Eq. (30) using a high value of the spring stiffness to represent a rigid connection.

Eq. (30) can be solved for each frequency and wavenumber to obtain the unknown reaction forces $\tilde{\mathbf{P}}_{t_t}(\kappa_y,\omega)$ between the track and the tunnel. The track displacements $\tilde{\mathbf{u}}_{t_r}(\tilde{\mathbf{x}},\kappa_y,\omega)$, the tunnel displacements $\tilde{\mathbf{u}}_{t_t}(\tilde{\mathbf{x}},\kappa_y,\omega)$ and the soil displacements $\tilde{\mathbf{u}}_s(\tilde{\mathbf{x}},\kappa_y,\omega)$ are then calculated using Eqs. (28), (26) and (27), respectively. The track–tunnel–soil

displacements correspond to the transfer function $\tilde{h}_{zi}(\tilde{y}',\tilde{y},\kappa_y,\omega)$ in Eq. (19) required for computing the response to moving load.

5. The wheel–track interaction forces

The ground-borne vibrations from moving trains can be attributed to various excitation mechanisms. A distinction is made between the quasi-static and dynamic contribution, decomposing the time history $g_k(t)=g_{ks}+g_{kd}(t)$ of each axle load into a static component g_{ks} and a dynamic component $g_{kd}(t)$.

5.1. Quasi-static forces

The quasi-static excitation occurs when successive axles of the train pass over the track and can be modelled as constant forces moving along the track with the train speed v. The static load g_{ks} is equal to the axle weight w_k. The Fourier transform $\hat{g}_{ks}(\omega)$ equals $2\pi w_k\delta(\omega)$. The frequency content of the free field displacements is obtained by substituting $\hat{g}_k(\tilde{\omega})$ in Eq. (18) for periodic domains:

$$\hat{u}_i(\tilde{y}+nL,\omega)=\left[\sum_{k=1}^{n_a} w_k\exp\left(\mathrm{i}\frac{\omega}{v}y_{k0}\right)\right]\left[\frac{1}{v}\int_{-L/2}^{L/2}\exp\left(-\mathrm{i}\frac{\omega}{v}\tilde{y}'\right)\tilde{h}_{zi}(\tilde{y}',\tilde{y},\kappa_y,\omega)\,\mathrm{d}\tilde{y}'\exp\left(-\mathrm{i}\frac{\omega}{v}nL\right)\right] \tag{32}$$

where $\kappa_y=\omega/v-2m\pi/L$ with $\kappa_y\in]-\pi/L,\pi/L[$ and m is an integer. In expression (32), the second factor between square brackets is the response due to a single unit axle load moving with a speed v and an initial position $y_{k0}=0$. The factor in front represents a modulation of the frequency content that is determined by the train composition and the train speed v.

The quasi-static effect is distinguishable close to the track and it contributes to the low frequency response in the range 0–20 Hz [40]. The importance of the quasi-static excitation in the free field can only be realized if the load speed is high compared to the wave velocities in the soil.

5.2. Dynamic loads

Rail and wheel unevenness is the most common source of excitation in generation of vibrations from underground railways.

The dynamic interaction between the train and the track is explained considering only the vertical component of the displacements. For the sake of brevity, the subscript z denoting the vertical component is omitted in the following. For each axle k the continuity of vertical displacements at the contact point between the axle and track can be written as

$$u_{ak}(t)=u_{rk}(t)+u_{w/rk}(t) \tag{33}$$

where $u_{ak}(t)$ is the displacement of the k-th axle, $u_{rk}(t)$ is the track displacement at the k-th axle position in the moving frame of reference and $u_{w/rk}(t)=u_{w/rk}(y_{k0}+vt)$ is the combined wheel/rail unevenness perceived by axle k.

5.2.1. Invariant tracks

If the track is invariant, a Fourier transform can be applied to Eq. (33) to express the compatibility of the displacements at the contact point in the frequency domain [30]:

$$\hat{u}_{ak}(\omega)=\hat{u}_{rk}(\omega)+\hat{u}_{w/rk}(\omega) \tag{34}$$

The frequency content $\hat{u}_{w/rk}(\omega)$ of the track unevenness is calculated from the wavenumber domain representation $\tilde{u}_{w/r}(k_y)$ of the unevenness $u_{w/r}(y)$:

$$\hat{u}_{w/rk}(\omega)=\frac{1}{v}\tilde{u}_{w/r}\left(-\frac{\omega}{v}\right)\exp\left(\mathrm{i}\omega\frac{y_{k0}}{v}\right) \tag{35}$$

The dynamic axle loads $\hat{\mathbf{g}}_d(\omega)$ arising due to the rail and wheel unevenness $\hat{\mathbf{u}}_{w/r}(\omega)$ are computed after solving the vehicle–track interaction problem [25,30]:

$$[\hat{\mathbf{C}}^v(\omega)+\hat{\mathbf{C}}^t(\omega)]\hat{\mathbf{g}}_d(\omega)=-\hat{\mathbf{u}}_{w/r}(\omega) \tag{36}$$

where $\hat{\mathbf{C}}^v$ is the vehicle compliance and $\hat{\mathbf{C}}^t(\omega)$ is the track compliance in the moving frame of reference. The element $\hat{C}^t_{lk}(\omega)$ of the track compliance represent the response of the track at the time dependent position of the l-th axle due to a unit impulse at axle k.

The track compliance $\hat{C}^t_{lk}(\omega)$ is calculated in the moving frame of reference [30]. The track compliance can be computed in a fixed frame of reference if the train speed is much less than the critical wave speeds in the track–tunnel–soil system. The rail unevenness is modelled as a stochastic process characterized by a single sided power spectral density (PSD) [25,30].

5.2.2. Periodic tracks

In case of periodic tracks, both parametric excitation and unevenness excitation occur. The parametric excitation arises when the moving wheels experience varying dynamic stiffness of the track. This occurs if the track is discretely supported on sleepers and also in the case of discontinuous floating slab tracks. The receptance variation in a periodic cell generates an oscillating load at harmonics of the frequency $f_s = v/L$, where L is the period of the track and v is the speed of the train.

A measured acceleration spectrum near a railway track presented by Heckl et al. [41] shows that peaks appear at distinctive frequencies such as the sleeper passage frequency $f_s = v/L$. The parametric excitation has been studied previously by Nordborg [31,32], Sheng et al. [42], Takemiya et al. [43] and Metrikine et al. [44]. The modelling of parametric excitation described in the present paper is inspired by the work of Nordborg [31,32]. The methodology to compute dynamic forces accounting for the parametric excitation and the unevenness excitation is elaborated in the following.

The parametric excitation becomes important if the variation in the track receptance along the reference cell is not small. Studies have shown that the parametric excitation also becomes critical when the fundamental frequency $f_s = v/L$ coincides with the wheel–track resonance frequency [45]. The variation in the reference cell is important particularly in the case of discontinuous floating slab tracks as will be demonstrated in Section 6.

If the variation of the track receptance in the reference cell is small, then the dynamic forces $\hat{\mathbf{g}}_d(\omega)$ due to unevenness $\hat{\mathbf{u}}_{w/r}(\omega)$ can be calculated with reasonable accuracy using Eq. (36).

In case of a periodic structure, the vehicle–track interaction problem can be solved in the frequency domain, assuming that the unevenness is periodic. In the following, the track unevenness is assumed periodic with the period L_r equal to an integer multiple N of the spatial period L. A similar idea has also been used by Sheng et al. [33] to study the interaction between the moving vehicle and periodically supported tracks. In the following analysis, it is assumed that the response at $y = 0$ is not influenced by the track unevenness outside the zone $[-L_r/2, L_r/2]$. The track unevenness $u_{w/rk}(t)$ perceived by the k-th axle can be written in terms of the Fourier series:

$$u_{w/rk}(t) = \sum_{m=-\infty}^{\infty} r_m \exp\left(\mathrm{i}\frac{2\pi m}{L_r}(y_{k0} + vt)\right) = \sum_{m=-\infty}^{\infty} r_m \exp(\mathrm{i}\omega_m t)\exp\left(\mathrm{i}\frac{\omega_m}{v} y_{k0}\right) \tag{37}$$

where $\omega_m = 2\pi m v/L_r$ and r_m are the Fourier coefficients. The displacement of the k-th axle at the contact point is also periodic and can be written in terms of the Fourier series:

$$u_{ak}(t) = \sum_{m=-\infty}^{\infty} b_m^k \exp(\mathrm{i}\omega_m t) \tag{38}$$

The axle load $g_k(t)$ between the k-th axle and the track is written using the vehicle compliance and the vehicle displacement:

$$g_k(t) = w_k - \sum_{m=-\infty}^{\infty} \hat{C}_k^v(\omega_m)^{-1} b_m^k \exp(\mathrm{i}\omega_m t) \tag{39}$$

where $\hat{C}_k^v(\omega)$ is the vehicle compliance of the k-th axle and gives the vehicle's displacement at the contact point due to a unit load. The contact force $g_k(t)$ consists of two parts; the static force which causes the quasi-static excitation due to the movement of the weight of the vehicle on the track and the dynamic component which includes the effect of inertia as well as the suspension systems of the bogie.

The displacement of the rail in the moving frame of reference due to this contact force is

$$u_{rk}(t) = \sum_{l=1}^{n_a} \left[w_l C_{kl}^t(t;0) - \sum_{m=-\infty}^{\infty} \hat{C}_l^v(\omega_m)^{-1} b_m^l C_{kl}^t(t;\omega_m) \right] \tag{40}$$

where $C_{kl}^t(t;\omega_m)$ is the response of the track at the time dependent position of the k-th axle due to a harmonic load $1\mathrm{e}^{\mathrm{i}\omega_m t}$ at the time-dependent position of the l-th axle. Hussein et al. [34] have proposed three methods to compute the response of discontinuous tracks in the moving frame of reference: the Fourier repeating unit method, the periodic Fourier method and the modified phase method. The method developed here is based on the Floquet transformation.

For the case of a moving harmonic load, the time history $g_l(t)$ of the l-th axle is equal to $1\mathrm{e}^{\mathrm{i}\overline{\omega}t}$. The frequency content of the loading is $\hat{g}_l(\omega) = 2\pi\delta(\omega - \overline{\omega})$. The response of the rail due to the moving harmonic load follows from Eq. (18):

$$\hat{u}_r(\tilde{y} + nL, \omega) = \frac{1}{v}\exp\left[-\mathrm{i}\left(\frac{\omega - \overline{\omega}}{v}\right)(nL - y_{l0})\right] \int_{-L/2}^{L/2} \exp\left[-\mathrm{i}\left(\frac{\omega - \overline{\omega}}{v}\right)\tilde{y}'\right] \tilde{h}_{zz}(\tilde{y}', \tilde{y}, \kappa_y, \omega)\,\mathrm{d}\tilde{y}' \tag{41}$$

where $\kappa_y = (\omega - \overline{\omega})/v - 2m\pi/L$. Performing an inverse Fourier transform with respect to ω gives the displacement $u_r(y,t)$ in the time domain. The response $C_{kl}^t(t;\overline{\omega})$ in the moving frame of reference is obtained by evaluating $u_r(y,t)$ at $y = \hat{y}_{kl} + y_{l0} + vt$, where $\hat{y}_{kl}$ is the distance between the k-th and l-th axle.

These track displacements $C_{kl}^t(t;\omega_m)$ are also periodic and can be expressed in the following form using a Fourier series:

$$C_{kl}^t(t;\omega_m) = \sum_{p=-\infty}^{\infty} a_{pm}^{kl} \exp(\mathrm{i}\omega_p t) \tag{42}$$

This equation simply states that the periodicity of the structure modulates the harmonic response. Invoking this Fourier series representation of the response $C^t_{kl}(t;\omega_m)$ of the rail in Eq. (40) gives

$$u_{rk}(t)=\sum_{l=1}^{n_a}\sum_{p=-\infty}^{\infty}\left[w_l a^{kl}_{p0}-\sum_{m=-\infty}^{\infty}\hat{C}^v_l(\omega_m)^{-1}b^l_m a^{kl}_{pm}\right]\exp(\mathrm{i}\omega_p t) \tag{43}$$

The above expression can be rearranged to give

$$u_{rk}(t)=\sum_{l=1}^{n_a}\sum_{m=-\infty}^{\infty}\left[w_l a^{kl}_{m0}-\sum_{p=-\infty}^{\infty}\hat{C}^v_l(\omega_p)^{-1}b^l_p a^{kl}_{mp}\right]\exp(\mathrm{i}\omega_m t) \tag{44}$$

Substituting the vehicle displacement and the rail displacement from Eqs. (38) and (44) in the compatibility Eq. (33) gives:

$$\sum_{m=-\infty}^{\infty}b^k_m\exp(\mathrm{i}\omega_m t)=\sum_{l=1}^{n_a}\sum_{m=-\infty}^{\infty}\left[w_l a^{kl}_{m0}-\sum_{p=-\infty}^{\infty}\hat{C}^v_l(\omega_p)^{-1}b^l_p a^{kl}_{mp}\right]\exp(\mathrm{i}\omega_m t)+\sum_{m=-\infty}^{\infty}r_m\exp\left(\mathrm{i}\frac{\omega_m}{v}y_{k0}\right)\exp(\mathrm{i}\omega_m t) \tag{45}$$

This results in the following relationship:

$$b^k_m=\sum_{l=1}^{n_a}\left[w_l a^{kl}_{m0}-\sum_{p=-\infty}^{\infty}\hat{C}^v_l(\omega_p)^{-1}b^l_p a^{kl}_{mp}\right]+r_m\exp\left(\mathrm{i}\frac{\omega_m}{v}y_{k0}\right)$$
$$\forall m=-\infty,\ldots,-1,0,1,\ldots,\infty \text{ and } \forall k=1,\ldots,n_a \tag{46}$$

This is an infinite system of linear equations, which can be solved to obtain the Fourier coefficients b^k_m of the vehicle's displacement. The number of terms to be considered depends on the fundamental frequency, the speed of the train, frequency components of the unevenness and the frequency range of interest. The Fourier coefficients of the vehicle displacement and the rail displacement satisfy the relation $b^k_m=b^{k*}_{-m}$, which can be utilized for an efficient implementation.

After the determination of the Fourier coefficients b^k_m, the total force $g_k(t)=g_{ks}+g_{kd}(t)$ is calculated from Eq. (39).

6. Numerical examples

The proposed methodology is used to analyze and compare the performance of continuous and discontinuous floating slab tracks as a vibration countermeasure.

An invariant circular tunnel embedded at a depth $d_t=20\,\mathrm{m}$ in a homogeneous half space is analyzed (Fig. 2). The tunnel has an internal radius $r_i=2.7\,\mathrm{m}$ and a wall thickness $t=0.3\,\mathrm{m}$. Hence, the outer radius of the tunnel or the radius r_e of the cavity is equal to 3.0 m. The tunnel is made of concrete with a Young's modulus $E_t=35\times10^9\,\mathrm{Pa}$, a Poisson's ratio $\nu_t=0.25$ and a density $\rho_t=2500\,\mathrm{kg/m^3}$. The concrete on the tunnel invert has a Young's modulus $E^t=28\,500\,\mathrm{MPa}$, a Poisson's ratio $\nu^t=0.2$ and a density $\rho^t=2500\,\mathrm{kg/m^3}$.

The half space has a shear wave velocity $C_s=250\,\mathrm{m/s}$, a longitudinal wave velocity $C_p=500\,\mathrm{m/s}$, a density $\rho_s=1750\,\mathrm{kg/m^3}$ and a hysteretic material damping ratio $\beta_s=\beta_p=0.025$ in shear and volumetric deformation. These properties are typical for a half space consisting of dry sand.

In the coupled FE–BE model, the infinitely long tunnel is reduced to a single bounded reference cell. Since an invariant tunnel is analyzed, the period L can arbitrarily be chosen as 0.3 m.

A finite element model of the reference cell is made using the general purpose finite element program ANSYS. The circular concrete lining of the tunnel is modelled with 8-node brick elements, including incompatible bending modes

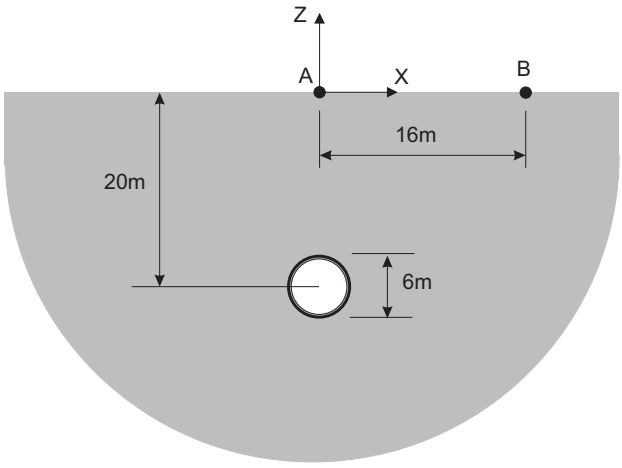

Fig. 2. Problem outline: tunnel embedded in a half space.

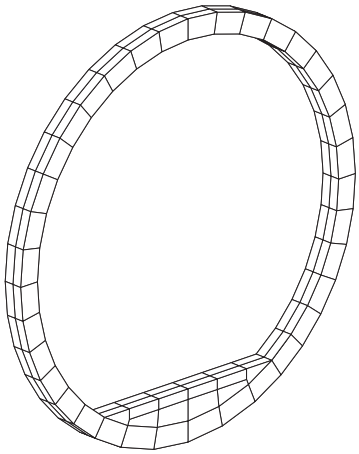

Fig. 3. Finite element model of the reference cell of the tunnel.

(Fig. 3). The size of the finite elements is governed by the boundary element mesh along the tunnel–soil interface, so that ideally a minimum of $N=8$ elements are used per shear wavelength $\lambda_s^{\min}=C_s/f_{\max}$, with $C_s=250\,\mathrm{m/s}$ the shear wave velocity in the soil and $f_{\max}=100\,\mathrm{Hz}$ the maximum excitation frequency. This results in a recommended element length $l_e=\lambda_s^{\min}/N=0.3125\,\mathrm{m}$. In the present model, two elements are used in the longitudinal direction ($l_e=0.15\,\mathrm{m}$), while 60 elements are used to model the tunnel lining in the circumferential direction ($l_e=0.31\,\mathrm{m}$).

The train consists of six cars each of length 19 m. The bogie and axle distances on all cars are 12.6 and 2.3 m, respectively. The total mass of the train is 342 ton, resulting in an axle load of 139.8 kN. The mass of the coach with passengers is 43 ton, while the mass of the bogie and axle are 3.6 and 1.7 ton, respectively. The speed of the train v is equal to 60 km/h. Since the train suspensions are important only at low frequencies, the vehicle compliance can be well approximated using the unsprung axle mass only. The vehicle compliance matrix $\hat{\mathbf{C}}^{v}(\omega)$ then is equal to $\mathrm{diag}\{-1/(M_u\omega^2)\}$.

Three track structures are considered in the tunnel: a direct fixation track, a continuous floating slab track and a discontinuous floating slab track. A direct fixation track is chosen as a reference case and the performance of continuous and discontinuous floating slab tracks as a vibration countermeasure is assessed.

6.1. Direct fixation track

A direct fixation track is considered in the tunnel. UIC 60 rails are used that have a cross-sectional area $A_r=7.672\times10^{-3}\,\mathrm{m}^2$, a moment of inertia $I_r=3.039\times10^{-5}\,\mathrm{m}^4$, a mass per unit length $\rho_r A_r=60.22\,\mathrm{kg/m}$ and a bending stiffness $E_rI_r=6.382\times10^{6}\,\mathrm{N\,m}^2$. Soft rail pads with a stiffness $k_{\mathrm{rp}}=70\,\mathrm{MN/m}$ discretely support the rails at an interval $d=0.6\,\mathrm{m}$ on the sleepers. The smeared stiffness of the rail pads is equal to $\overline{k}_{\mathrm{rp}}=k_{\mathrm{rp}}/d=116\,\mathrm{MN/m}^2$. The concrete sleepers are cast into the tunnel invert. The track is modelled as an infinite beam on discrete support. The model consists of an infinite Euler beam, representing the (two) rails and the mass elements representing the sleepers. The concrete sleepers are rigidly attached to the tunnel invert by means of very stiff springs below the mass elements.

The track is modelled as a periodic structure of length $L_2=0.6\,\mathrm{m}$. The common spatial period of the track and the tunnel is $L=L_2=2L_1=0.6\,\mathrm{m}$. The track structure is discretely connected to the tunnel invert at the positions of the sleepers. The track–tunnel–soil coupling is performed on a reference cell $\tilde{\Omega}$ of length $L=0.6\,\mathrm{m}$. The different spatial periods of the track and tunnel in this particular example are only chosen to demonstrate the applicability of the procedure. Alternatively, the Craig–Bampton substructuring could have been used to incorporate the track in the tunnel by choosing the spatial period of the tunnel equal to the sleeper distance of 0.6 m.

The track structure and the tunnel–soil systems are first solved separately on reference cells $\tilde{\Omega}_2$ and $\tilde{\Omega}_1$, respectively. The solution of both systems is expressed on a reference cell with the common spatial period and then the coupling is performed in the frequency–wavenumber domain as discussed in Section 4.

Fig. 4 shows the transfer functions at the rail, the tunnel invert and on the free surface at points A and B (Fig. 2). The response at the rail and the tunnel invert does not show any marked resonance in the frequency range 1–100 Hz due to tunnel–soil interaction. The response in the free surface exhibits an undulating behavior due to the interference of the compression and shear or Rayleigh waves. These transfer functions have been checked with the approach based on the Craig–Bampton substructuring.

To compute the response to moving loads, two excitation mechanisms have been considered: the quasi-static excitation and the unevenness excitation. The parametric excitation due to sleeper periodicity is ignored as the variation in the track receptance in the sleeper bay is small and the sleeper passage frequency $f_s=v/L=27\,\mathrm{Hz}$ does not coincide with the

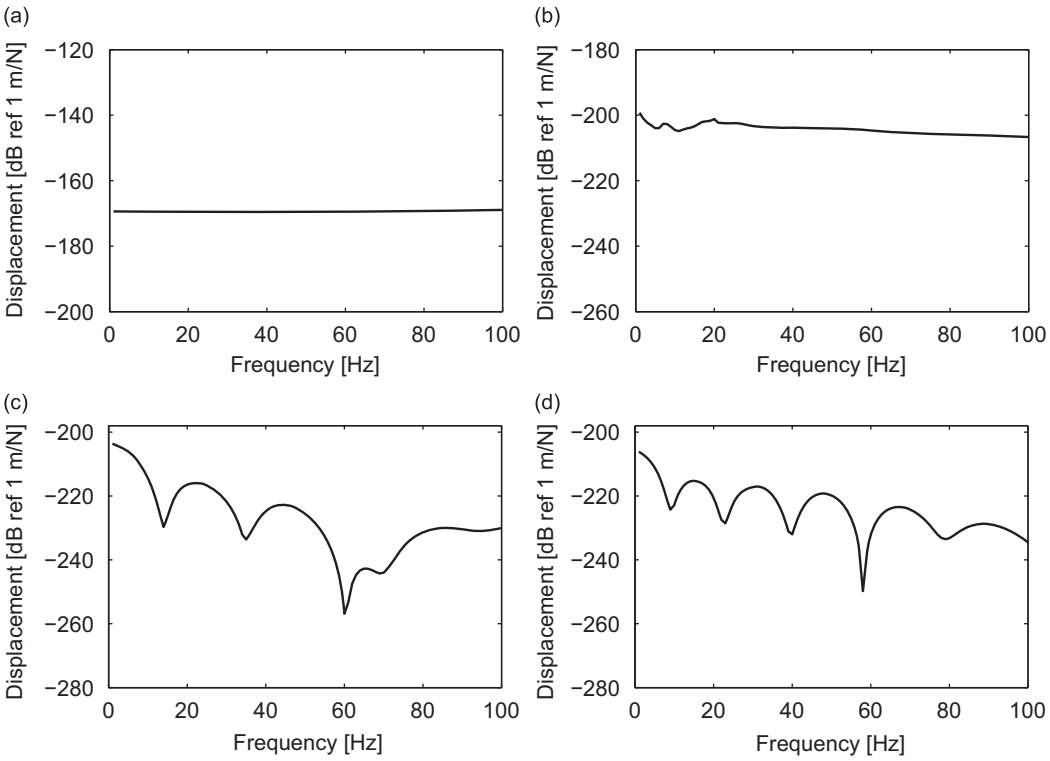

Fig. 4. Vertical transfer function at (a) the rail, (b) the tunnel invert and in the free field at points (c) A and (d) B.

Table 1
Roughness parameter for FRA track classes.

Track class	6	5	4	3	2	1
A' (10^{-7} m cycle)	1.06	1.69	2.96	5.29	9.52	16.72

wheel/track resonance frequency. Thus, the approach for invariant tracks can be adopted to calculate the dynamic forces due to unevenness excitation.

Theoretically, the rail unevenness $u_{w/r}(y)$ is modelled as a stochastic process characterized by the power spectral density (PSD) functions. Several PSD curves to describe rail unevenness are available in the literature. The analytical expression of the power spectral density of track irregularities is given in various empirical forms. These relations are usually expressed in terms of the one-sided power spectral density $\tilde{G}'(n_y)$ or $\tilde{G}(k_y)$ given as a function of the cyclic wavenumber $n_y = 1/\lambda_y$ or wavenumber k_y.

On the basis of extensive measurements on the US railway network, the following empirical relation has been devised by the Federal Railroad Administration (FRA) [25,46]:

$$\tilde{G}'_{w/r}(n_y) = \frac{A' n_{y2}^2 (n_y^2 + n_{y1}^2)}{n_y^4 (n_y^2 + n_{y2}^2)} \tag{47}$$

Depending on the rail quality, the track is divided into six classes according to the FRA, class 6 track being the best and class 1 the poorest. $n_{y1} = 0.0233$ cycle/m and $n_{y2} = 0.1312$ cycle/m are the break frequencies that do not change significantly for different track classes. The unevenness parameter A' is strongly dependent on the track class and its values are summarized in Table 1.

In this paper, FRA track class 6 is used for which the unevenness parameter $A' = 1.06 \times 10^{-7}$ m cycle [25,46]. An artificial unevenness profile is generated from this PSD curve and the frequency content of unevenness is determined for a speed of 60 km/h [25,30].

Since the parametric excitation is disregarded, Eq. (36) for invariant tracks can be used to calculate the dynamic forces. Fig. 5 shows the frequency content and one-third octave band RMS spectrum of the contact force on the front axle of the train. The maximum force appears at the vehicle–track resonance frequency of about 70 Hz.

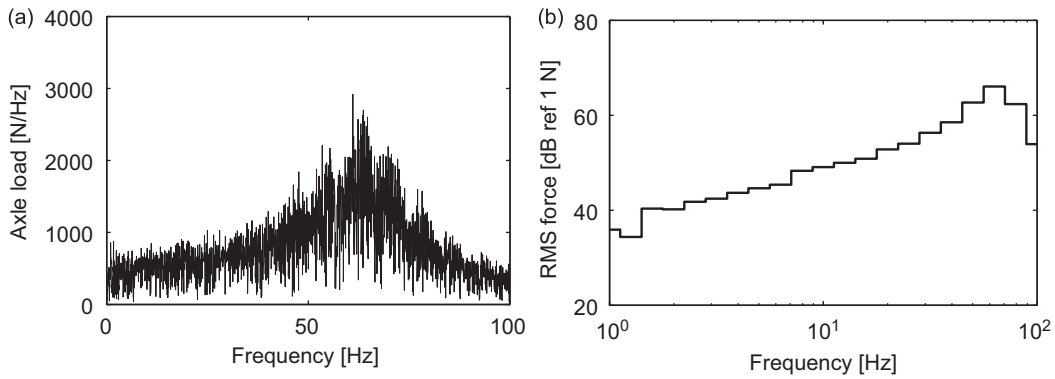

Fig. 5. (a) Frequency content and (b) one-third octave band RMS spectrum of the contact force at the front axle of the train due to unevenness excitation.

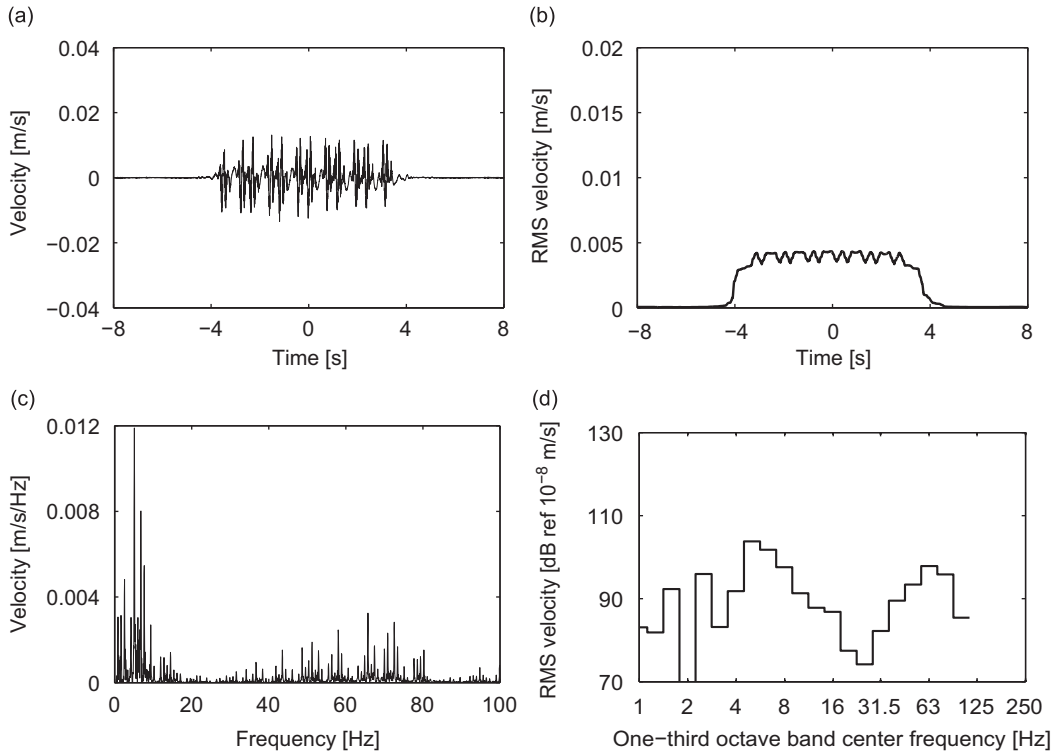

Fig. 6. (a) Time history, (b) running RMS, (c) frequency content and (d) one-third octave band RMS spectrum of the vertical velocity at the rail due to the passage of a train in the tunnel at a speed of 60 km/h.

Fig. 6 shows the time history, running RMS, frequency content and the one-third octave band RMS spectrum of the vertical velocity on the rail. At low frequencies below 10 Hz, the response on the rail is dominated by the quasi-static forces and, as a result, the passage of individual axles of the train can be distinguished in the time history. Above 30 Hz the dynamic forces due to rail unevenness are contributing to the response, but their influence remains lower than the quasi-static forces.

Fig. 7 shows the time history, running RMS, frequency content and one-third octave band RMS spectrum of the vertical velocity on the tunnel invert. The effect of the quasi-static forces on the tunnel has shifted to lower frequencies and is less pronounced than on the rail. The effect of the dynamic forces is comparable to that the quasi-static forces on the tunnel invert. Figs. 8 and 9 show the response in the free field at points A and B. The contribution of the quasi-static forces has further reduced in the free field as the evanescent waves generated by the quasi-static excitation decay significantly. The distance between the point A and the tunnel is less than the wavelength of the shear waves in the soil at a frequency of 10 Hz. Thus, some contribution of the quasi-static forces below 10 Hz is observed at point A. At point B, which is located further away from the tunnel the effect of the quasi-static forces is negligible. The maximum response in the free field is observed around the wheel–track resonance frequency of 70 Hz due to rail unevenness. The passage of the individual axles

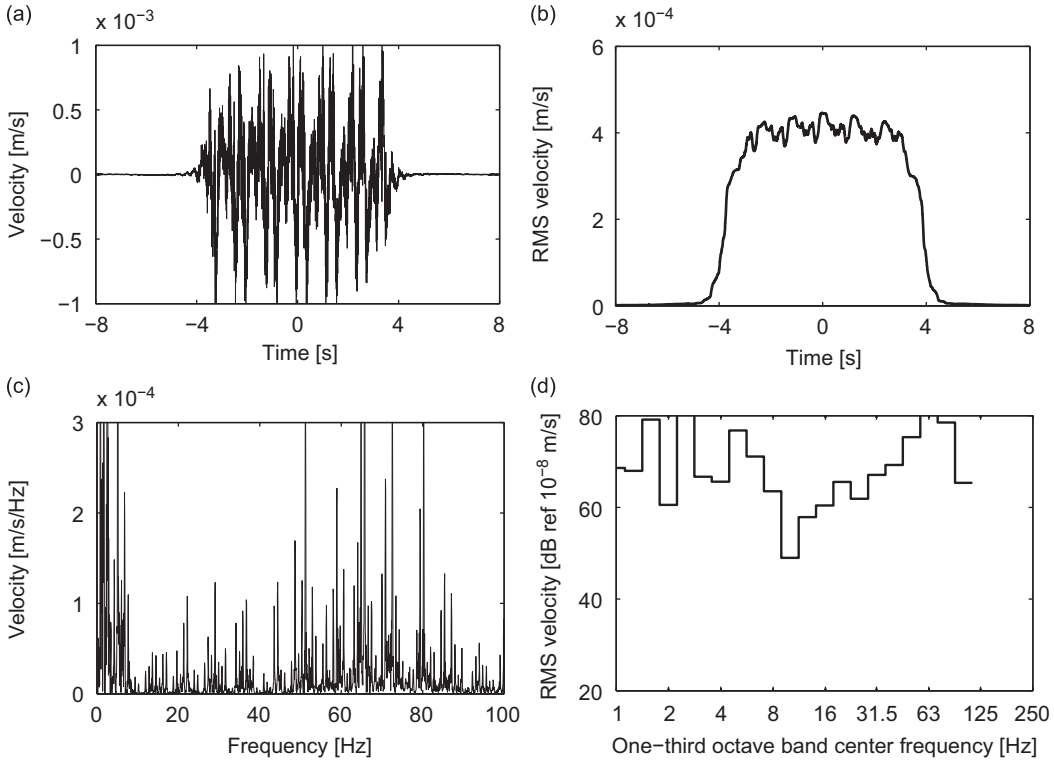

Fig. 7. (a) Time history, (b) running RMS, (c) frequency content and (d) one-third octave band RMS spectrum of the vertical velocity at the tunnel invert due to the passage of a train in the tunnel at a speed of 60 km/h.

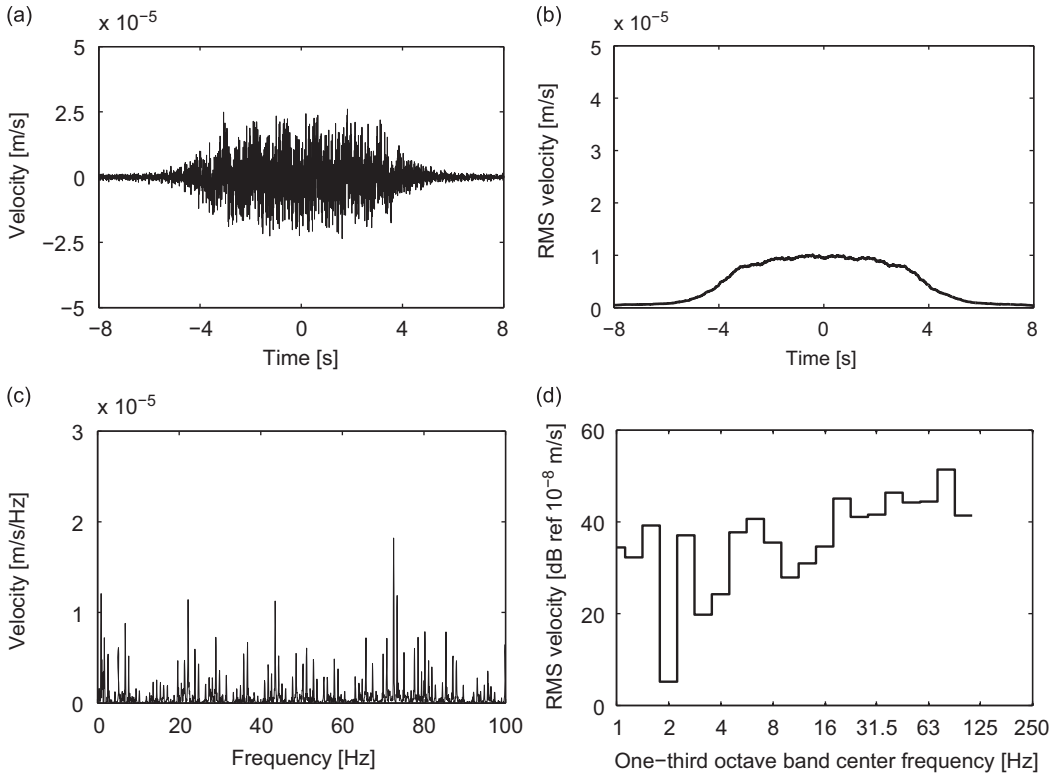

Fig. 8. (a) Time history, (b) running RMS, (c) frequency content and (d) one-third octave band RMS spectrum of the vertical velocity in the free field at point A due to the passage of a train in the tunnel at a speed of 60 km/h.

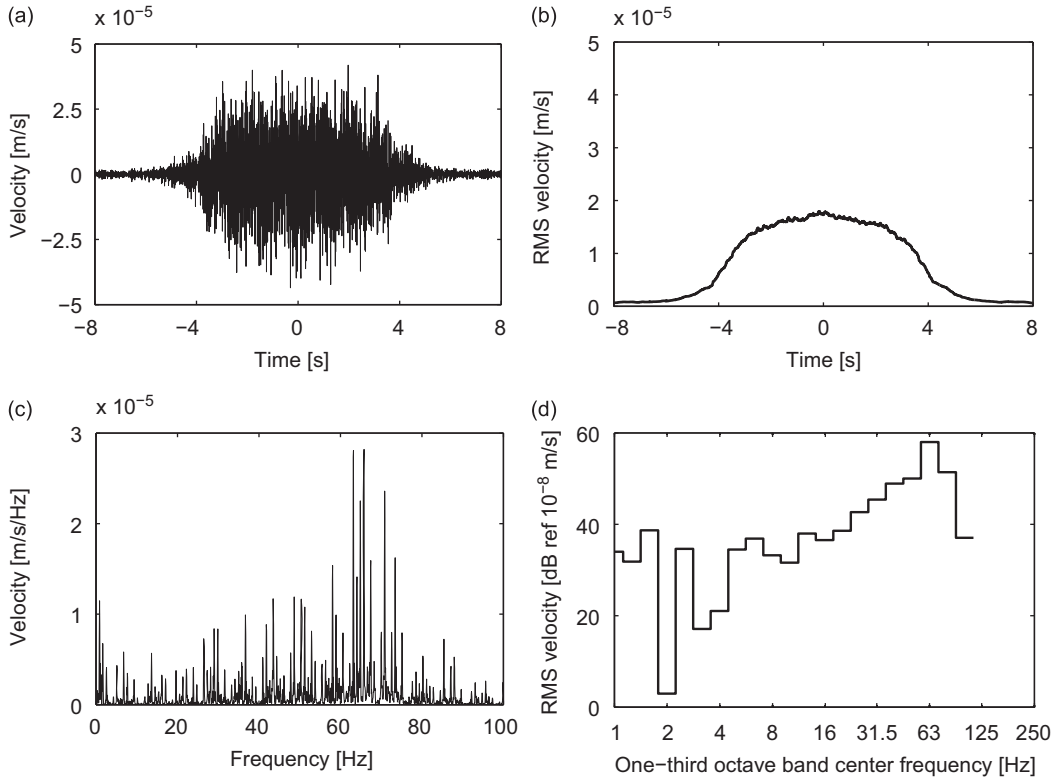

Fig. 9. (a) Time history, (b) running RMS, (c) frequency content and (d) one-third octave band RMS spectrum of the vertical velocity in the free field at point B due to the passage of a train in the tunnel at a speed of 60 km/h.

of the train is not clearly distinguishable in the time history of the free field response. It may be noted that the response at a lateral distance of 16 m from the tunnel (point B) is higher than the response directly above the tunnel (point A). This is a consequence of waves emanating to the side of the tunnel and eventually reaching the surface at some lateral distance from the tunnel axis.

6.2. Floating slab track

Floating slab track (FST) is widely used as a vibration isolation measure in tunnels. The FST consists of a concrete slab, which is coupled to the tunnel invert via resilient bearings. The rails are supported on the concrete slab by means of the rail pads.

FST systems can be classified into two types: continuous FST and discontinuous FST. Continuous FST systems are formed by casting the concrete slab in situ, while discontinuous FST systems use pre-cast concrete sections of finite length (typically 6 m). A disadvantage of discontinuous FST systems is that, as there is no transfer of shear forces between adjacent slabs, the rail and the fastening system bear additional forces and rail fracture is more likely to occur [47]. To allow the transfer of the shear force through the slabs, practitioners recommend the use of shear connections between adjacent slabs. Stiffer bearings near the joints of consecutive slabs are also used to prevent excessive deflections [47]. Advantages of using discontinuous slabs over continuous slabs are easy maintenance and replaceability.

In this paper, the vibration isolation efficiency of a floating slab track with an isolation frequency of 10 Hz is investigated. Both continuous and discontinuous slabs are considered and their vibration isolation efficiency is compared.

Discontinuous concrete slabs with a length of 6 m, a width of 2.7 m and a height of 0.505 m are supported by two rows of 5 springs with a spring stiffness of $K_{sb} = 8.1$ MN/m (Fig. 10). The slab has a bending stiffness $E_{sl}I_{sl} = 941.7 \times 10^6$ N m^2 and a mass per unit length $\rho_{sl}A_{sl} = 3340.6$ kg/m. If this system is idealized as a single degree-of-freedom system it has an isolation frequency of 10 Hz. The characteristics of the 10 Hz FST are realistic and represent one of the track designs in Beijing metro. The rails are discretely supported on rail pads at an interval of 0.6 m. The properties of the rail and the rail pads are the same as used in Section 6.1.

The track is modelled as a periodic structure of length $L_2 = 6$ m, while the tunnel is modelled as a periodic structure of length $L_1 = 0.3$ m. The common spatial period of the track and the tunnel is $L = L_2 = 20L_1 = 6$ m. The track structure is discretely connected to the tunnel invert at the positions of the resilient bearings. To model the continuous floating slab track, periodic boundary conditions are imposed on the degrees of freedom of the rail and the slab at the ends of the

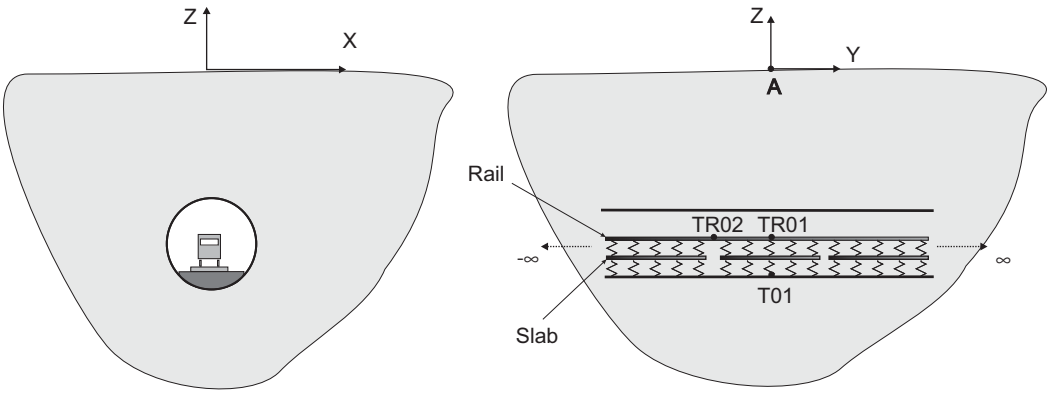

Fig. 10. Discontinuous floating slab track in the tunnel.

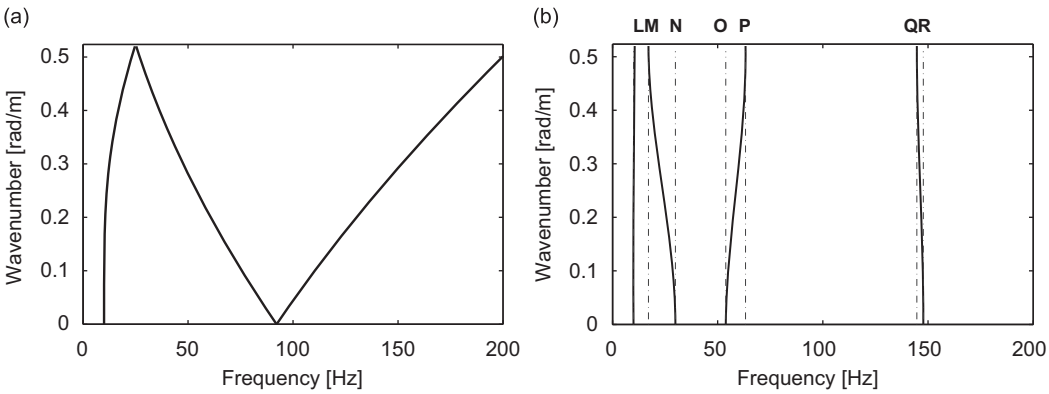

Fig. 11. Dispersion curves of (a) the continuous and (b) the discontinuous floating slab track.

reference cell. In the case of the discontinuous floating slab track, the periodic boundary conditions are only imposed on the degrees of freedom of the rail at the end of the reference cell, while the two ends of the slab are free such that the shear force and bending moment are equal to zero.

A periodic FE approach is used to model both track systems. The dynamic stiffness matrix characterizing the slab bearings is a diagonal matrix $\tilde{\mathbf{K}}_{sb} = \mathrm{diag}\{2K_{sb}\}$ of order 5. The hysteretic damping factor of the slab bearings is $\eta_s = 0.2$. The coupling between the track and the tunnel is performed as described in Section 4 to calculate the transfer function.

6.2.1. Transfer functions of continuous and discontinuous FST

Fig. 11 displays the dispersion curves of the continuous and discontinuous floating slab track. The dispersion curves are shown in the Floquet domain for positive wavenumbers in the range $[0, \pi/L]$. Above the cut-on frequency of 10 Hz, the bending wave in the continuous track can freely propagate. The discontinuity in the slab leads to the formation of stop bands (Fig. 11b). The bounding frequencies of the pass and stop bands can be found by calculating the natural frequencies of the periodic unit after imposing the appropriate boundary conditions. The lower frequency bounds of the propagation zone at $\kappa = 0$ can be calculated by imposing the displacements and rotations of the rail to be equal, while the upper frequency bounds at $\kappa = \pi/L$ can be calculated by imposing the displacements and rotations to be equal but out-of-phase. The second pass band (M–N) between 17 and 29 Hz corresponds to the pitching movement of the slab. The pass bands around 55 Hz (O–P) and 147 Hz (Q–R) correspond to the first and second bending modes of the slab with free boundary conditions at the ends.

Fig. 12 shows the transfer functions at the rail, the tunnel invert and in the free field at points A and B. In case of the discontinuous floating slab track, the observation point on the rail is chosen directly above the slab discontinuity. The first peak at 10 Hz in the transfer functions of the continuous as well as the discontinuous floating slab tracks corresponds to the resonance of the slab on the resilient bearings. An additional peak at 55 Hz appears for the case of the discontinuous slab and is attributed to the formation of the standing wave in the slab. This resonance effect is not pronounced in the free field, and the transfer functions in the free field are similar for the continuous and discontinuous floating slab tracks. This is in contrast to the dispersion curves for the two cases, which are quite different. The dispersion curves shown in Fig. 11 give an

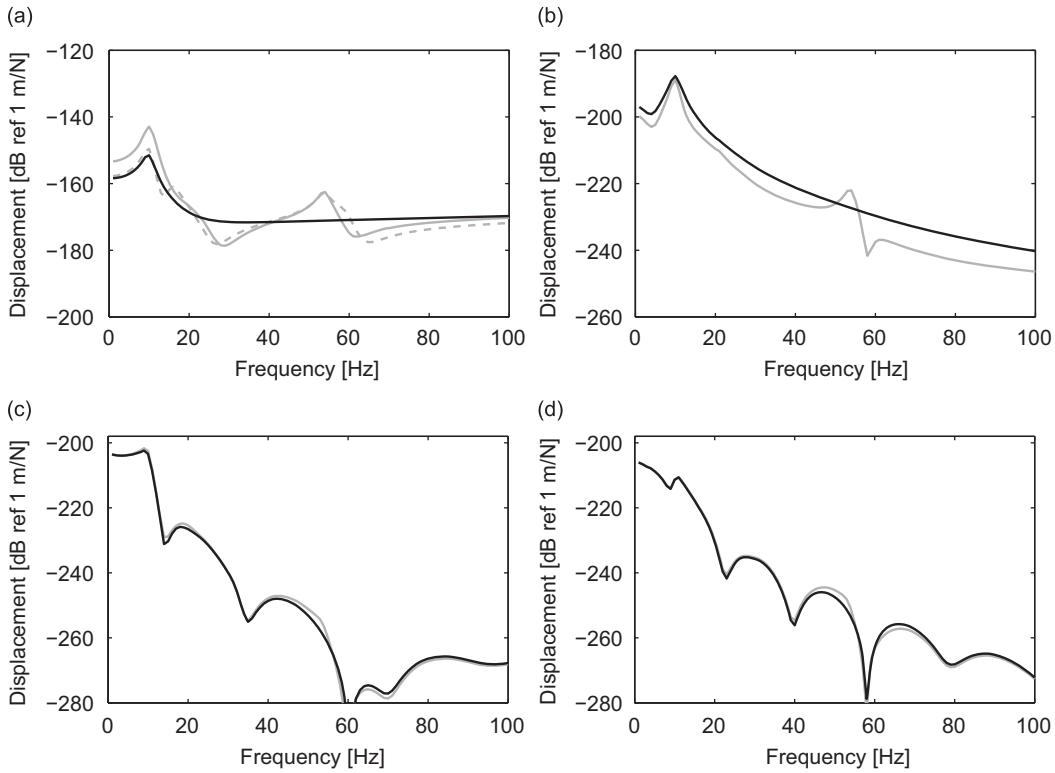

Fig. 12. Vertical transfer function at (a) the rail (TR02), (b) the tunnel invert (T01) and in the free field at points (c) A and (d) B due to a load on the rail at TR02 for a continuous (black line) and a discontinuous (gray solid line) floating slab track. Superimposed on (a) is the rail receptance at the center of the discontinuous slab TR01 (gray dashed line).

insight into the wave propagation along the track, while the response in the free field is mainly due to waves propagating perpendicular to the tunnel. Superimposed on Fig. 12 a is also the rail receptance of the discontinuous slab track at the center of the slab. The difference in the rail receptance at the center and the end of the slab is evident from the figure. The rail receptance of the continuous floating slab track is closer to the rail receptance at the center of the discontinuous slab, particularly at low frequencies up to 15 Hz.

6.2.2. Axle loads on continuous and discontinuous FST

In the following, the quasi-static excitation and unevenness excitation due to the passage of a train on continuous and discontinuous FSTs is considered. In case of a discontinuous floating slab track, parametric excitation will occur due to receptance variation along the slab.

Hussein and Hunt [34,36] have studied the effect of parametric excitation and found that the force at the wheel–rail interface only increased by 1% of its static value due to slab discontinuity. In this paper, the variation in the unevenness excitation and the quasi-static excitation due to slab discontinuity as well as parametric excitation are discussed. Since the stiffness of the bearings is much less than the stiffness of the track bed, the track can be assumed to be on a rigid base in order to calculate the track receptance $\mathbf{C}^t(t;\omega_m)$. A semi-analytical procedure based on the Floquet transform is used to compute the receptance of the discontinuous floating slab track. It is also possible to calculate the track receptance from the periodic finite element model of the track. It is faster, however, to calculate the track compliance and the Fourier coefficients a_{kl}^{pm} in the case of the periodic track using a semi-analytical formulation. This approach is outlined in Appendix B.

The floating slab track is modelled as a double beam on an elastic foundation [48]. The stiffness of the rail pads and the slab bearings are smeared in the longitudinal direction. The smeared stiffness of the rail pads is $\overline{k}_{\mathrm{rp}} = 116\,\mathrm{MN/m^2}$, while that of the slab bearings is $\overline{k}_{\mathrm{sb}} = 10K_{\mathrm{sb}}/L = 13.5\,\mathrm{MN/m^2}$.

Fig. 13 shows the real and the imaginary part of the rail displacement $C_{kk}^t(t;\omega_m)$ under the load in the moving frame of reference due to a moving harmonic load $1\exp(\mathrm{i}2\pi 5t)$ on the continuous and discontinuous floating slab at a speed of $v = 60\,\mathrm{km/h}$. The rail response is displayed over a length of 12 m on the track from $y = [-6\,\mathrm{m}, 6\,\mathrm{m}]$. The wavelength of the response corresponds to the excitation frequency of the harmonic load. The Doppler effect is not visible as the speed of the load is considerably less than the critical speed of the system. In case of the continuous floating slab track, the amplitude of the track receptance is constant along the slab. For the discontinuous floating slab track the variation along the slab $y = [-3\,\mathrm{m}, 3\,\mathrm{m}]$ can be observed. Fig. 14 shows the rail displacements in the moving frame of reference due to the moving

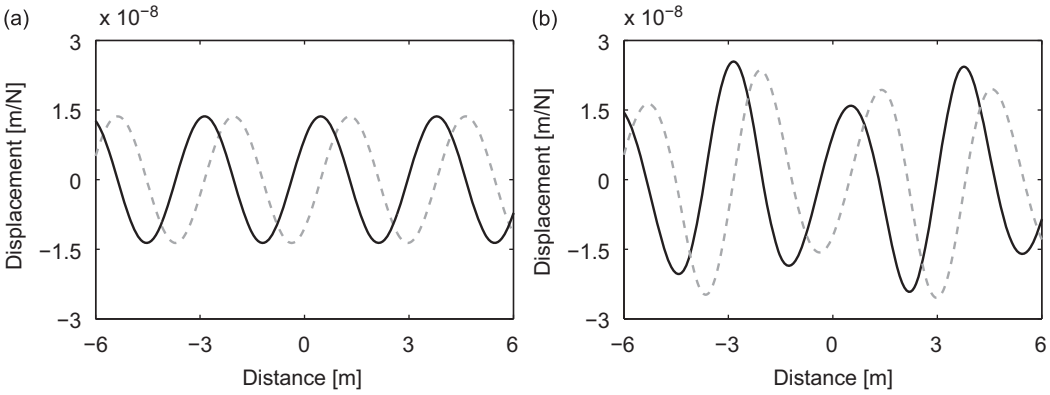

Fig. 13. Real (black line) and imaginary (gray line) part of the rail displacement under the load in the moving frame of reference due to a moving unit harmonic load at 5 Hz on (a) a continuous and (b) a discontinuous floating slab track at a speed of 60 km/h.

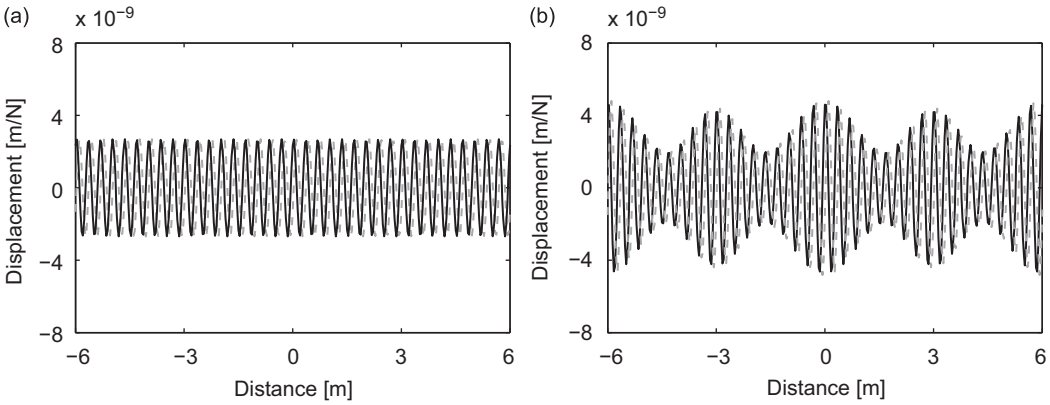

Fig. 14. Real (black line) and imaginary (gray line) part of the rail displacement under the load in the moving frame of reference due to a moving unit harmonic load at 50 Hz on (a) a continuous and (b) a discontinuous floating slab track at a speed of 60 km/h.

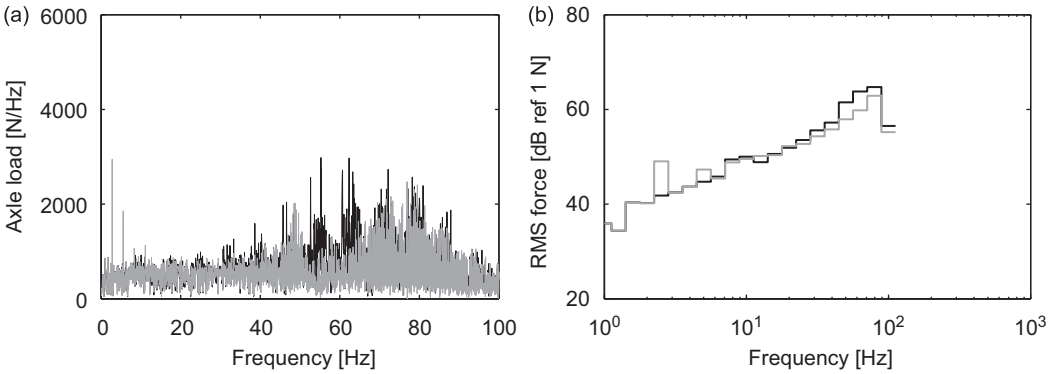

Fig. 15. (a) Frequency content and (b) one-third octave band RMS spectrum of the front axle load for the case of a continuous (black line) and a discontinuous (gray line) floating slab track.

harmonic load $1\exp(i2\pi 50t)$. The wavelength of the response has decreased in accordance with the increase of the excitation frequency. The modulation of the harmonic response due to the periodicity of the structure is clearly visible in the case of the discontinuous floating slab track.

Fig. 15 compares the frequency content and one-third octave band RMS spectrum of the contact force at the front axle of the train for the case of continuous and discontinuous FST. The maximum force appears at the vehicle–track resonance frequency, which still lies between 60 and 90 Hz. The dynamic component of the forces at the wheel–track resonance are

higher for the continuous FST than for the discontinuous FST. This is due to the fact that the decay rate on the continuous floating slab track is low. This results in a strong coupling between different axles of the train and gives rise to higher interaction forces. For the discontinuous FST, the decay rates are high around the wheel–track resonance frequency due to the formation of a stop band (P–Q) between 55 and 147 Hz in the periodic structure. The resonance frequency of 55 Hz lies in a pass band and the waves can freely propagate at this frequency resulting in a higher magnitude of the dynamic force. Coincidence of the wheel–track resonance frequency with the resonance frequency of the slab should be avoided when designing a discontinuous FST. In case of discontinuous FST, peaks are also observed at the first two harmonics of the slab passage frequency $f_s = v/L = 2.78$ Hz. The magnitude of the dynamic force due to parametric excitation is comparable to the magnitude of the unevenness force around the wheel–track resonance frequency.

6.2.3. Response due to passage of train on a FST

Figs. 16–19 show the time history, running RMS, frequency content and one-third octave band RMS spectrum of the vertical velocity at the rail, the tunnel invert and in the free field at points A and B. The contribution of the quasi-static excitation is only noticeable at low frequencies below 10 Hz and is confined to the vicinity of the track. The response on the rail is dominated by quasi-static forces, which is greater in the case of the discontinuous FST due to an increase in the static track receptance. The dominant frequency content of the response on the tunnel invert is below 20 Hz as the track is isolated from the tunnel at higher frequencies. The contribution of dynamic forces around the wheel–track resonance frequency due to track unevenness has considerably diminished. However, the effect of dynamic forces due to parametric excitation in the case of discontinuous FST is distinguishable at the harmonics of the slab passage frequencies $f_s = v/L = 2.78$ Hz, which lie below the resonance frequency of the slabs. This particular effect is quite pronounced and leads to higher vibration levels in the free field in the low frequency range. As the higher frequency components are significantly attenuated on the tunnel invert and the slab, the resonance of the discontinuous slab at 55 Hz is not important for the free field response. In the present analysis, it has been observed that dynamic forces due to train–track interaction do not cause a prominent response at the natural frequency corresponding to the bending of the slab with free ends.

The vibration isolation efficiency of continuous and discontinuous floating slab tracks is compared by calculating the insertion gain in dB. The insertion gain is defined as the ratio of the response u^{iso} of the isolated and the response u^{uniso} of the unisolated system:

$$\text{IG[dB]} = 20\log\left(\frac{u^{\text{iso}}}{u^{\text{uniso}}}\right) \tag{48}$$

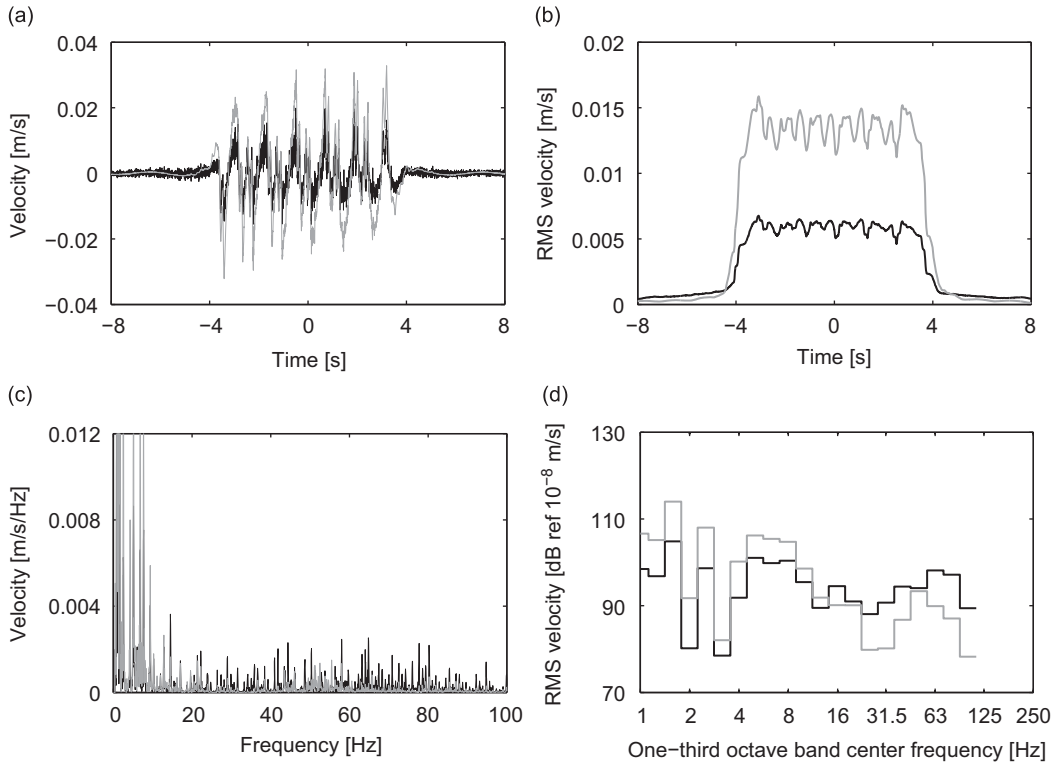

Fig. 16. (a) Time history, (b) running RMS, (c) frequency content and (c) one-third octave band RMS spectrum of the vertical velocity at the rail due to the passage of a train on a continuous (black line) and a discontinuous (gray line) floating slab track at a speed of 60 km/h.

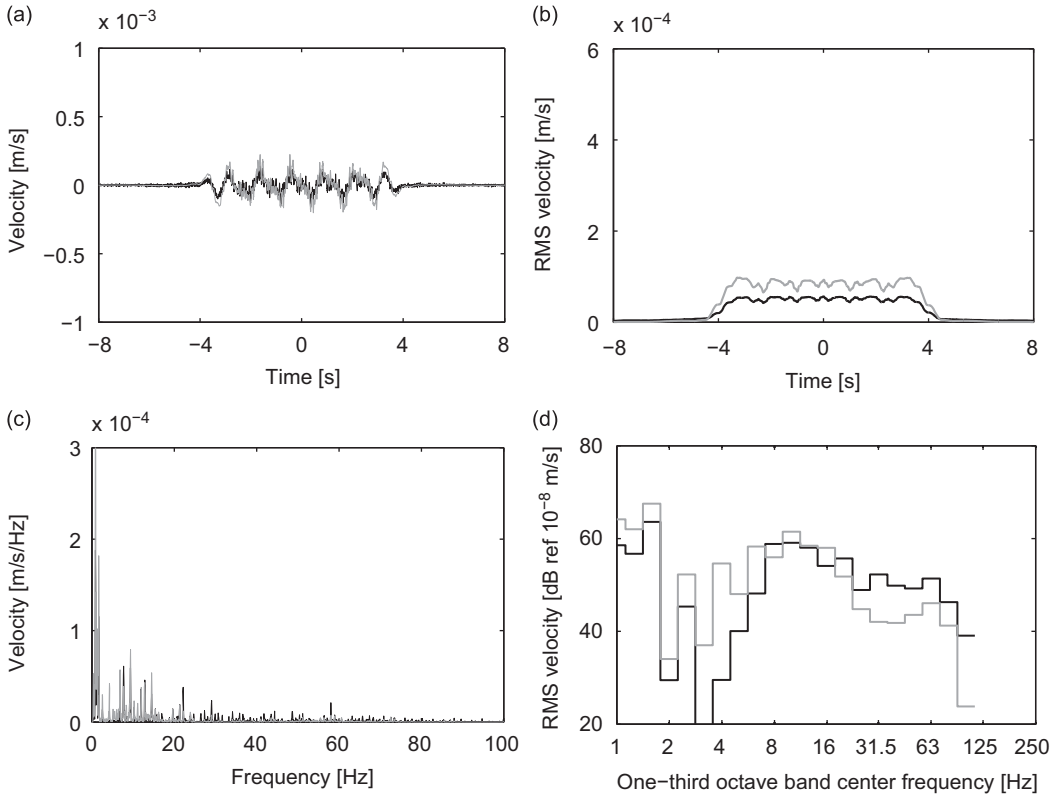

Fig. 17. (a) Time history, (b) running RMS, (c) frequency content and (d) one-third octave band RMS spectrum of the vertical velocity at the tunnel invert due to the passage of a train on a continuous (black line) and a discontinuous (gray line) floating slab track at a speed of 60 km/h.

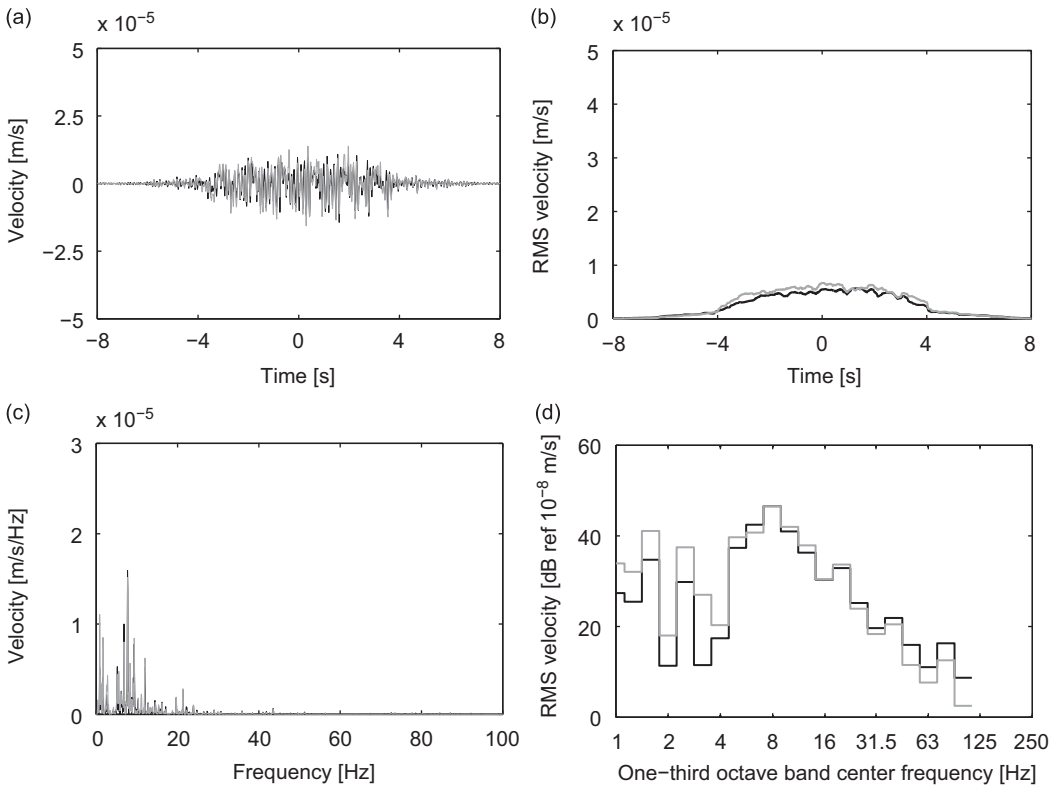

Fig. 18. (a) Time history, (b) running RMS, (c) frequency content and (d) one-third octave band RMS spectrum of the vertical velocity in the free field at point A due to the passage of a train on a continuous (black line) and a discontinuous (gray line) floating slab track at a speed of 60 km/h.

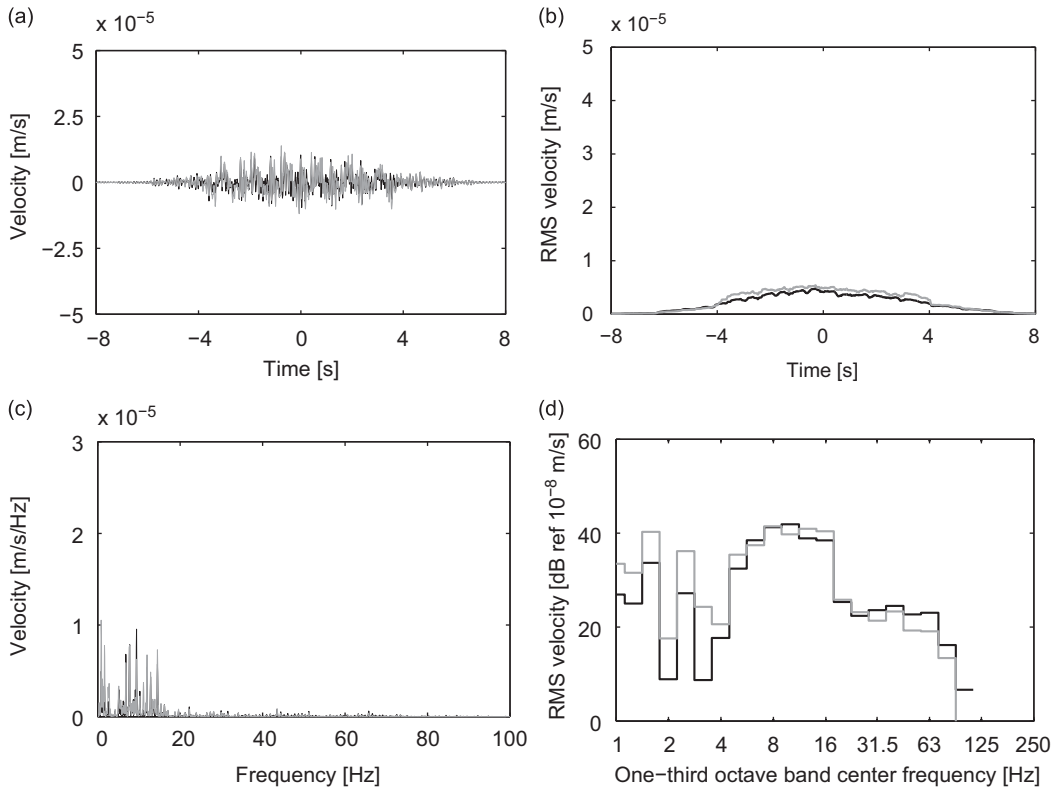

Fig. 19. (a) Time history, (b) running RMS, (c) frequency content and (d) one-third octave band RMS spectrum of the vertical velocity in the free field at point B due to the passage of a train on a continuous (black line) and a discontinuous (gray line) floating slab track at a speed of 60 km/h.

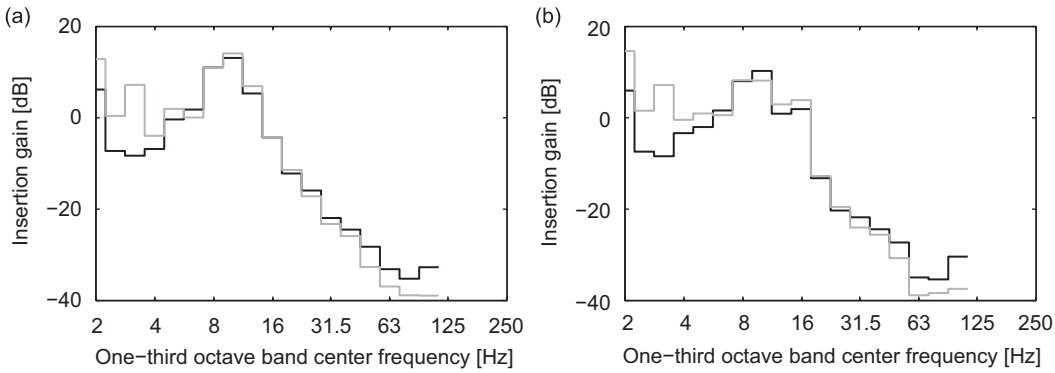

Fig. 20. Insertion gain in the free field at points (a) A and (b) B for the case of the continuous (black line) and discontinuous (gray line) floating slab tracks.

Fig. 20 shows the insertion gain on the free surface at a points A and B for the case of the continuous and discontinuous floating slab tracks. Negative values of the insertion gain imply vibration isolation.

The continuous and the discontinuous floating slab tracks behave in a similar manner at higher frequencies and no significant difference is observed between their performance as a vibration countermeasure. However, other practically aspects (robustness, maintenance etc.) must be considered while deciding which track system should be installed. Attention should also be given to low frequency response when designing the discontinuous slab tracks.

7. Conclusions

This paper has outlined a periodic approach based on the Floquet transform and its properties to couple a track and the tunnel–soil system of different periodicity. The general methodology for computing the transfer functions of the coupled track–tunnel–soil system as well as the computation of the dynamic force accounting for the interaction between the

moving vehicle and a periodic track are described. The methodology has been used to compare the efficiency of continuous and discontinuous FSTs. The following conclusions can be drawn from this analysis:

- The influence of the slab discontinuity on the rail receptance is quite significant compared to the effect on the transfer functions in the free field. The isolation efficiency of the continuous and discontinuous floating slab tracks differs primarily because of the vehicle–track interaction, rather than a modification of the transfer functions.
- Slab discontinuity causes variation in the rail receptance in the reference cell as well as leads to the creation of stop bands. This significantly influences the dynamic interaction between the train and the track. The change in the axle load around the wheel–track resonance frequency due to slab discontinuity is observed to be less important than the parametric excitation. However, the importance of parametric excitation significantly depends on the magnitude of the static load and will vary for different vehicles. As the parametric excitation occurs at frequencies less than typical isolation frequencies of floating slabs (10 Hz in the present analysis), it can result in an amplification of the free field response at low frequencies. This effect is shown to be important by comparing the insertion gain for the continuous and discontinuous floating slab tracks.
- In case of discontinuous slab tracks, the effect of slab resonances due to the formation of standing waves is found to be less important in the free field. This is because these resonances occur at frequencies well above the isolation frequency of the slab and the frequency components are significantly attenuated. The performance of continuous and discontinuous floating slab tracks is similar at higher frequencies.

Acknowledgments

The results presented in this paper have been obtained within the frame of the SBO Project IWT 03175 "Structural damage due to dynamic excitation: a multi-disciplinary approach", funded by IWT Vlaanderen. This financial support is gratefully acknowledged.

Appendix A. Relation between the Fourier and the Floquet transform

In the present paper, the relationships between the Fourier and the Floquet transform have been exploited to relate the solution on two periodic domains. These relations are elaborated in this appendix. To express the Fourier transform $\tilde{\hat{\mathbf{H}}}(\tilde{\mathbf{x}}', k_y, \omega)$ in terms of the Floquet transform $\tilde{\mathbf{H}}(\tilde{\mathbf{x}}', \tilde{y}_1, \omega)$, let us begin with the definition of the Fourier transformation:

$$\tilde{\hat{\mathbf{H}}}(\tilde{\mathbf{x}}', k_y, \omega) = \int_{-\infty}^{\infty} \hat{\mathbf{H}}(\tilde{\mathbf{x}}', y, \omega)\exp(+\mathrm{i}k_y y)\,\mathrm{d}y = \sum_{n=-\infty}^{+\infty} \int_{nL_1}^{(n+1)L_1} \hat{\mathbf{H}}(\tilde{\mathbf{x}}', y, \omega)\exp(+\mathrm{i}k_y y)\,\mathrm{d}y \tag{A.1}$$

Taking $y = \tilde{y}_1 + nL_1$ leads to

$$\tilde{\hat{\mathbf{H}}}(\tilde{\mathbf{x}}', k_y, \omega) = \sum_{n=-\infty}^{+\infty} \int_0^{L_1} \hat{\mathbf{H}}(\tilde{\mathbf{x}}', \tilde{y}_1 + nL_1, \omega)\exp[+\mathrm{i}k_y(\tilde{y}_1 + nL_1)]\,\mathrm{d}\tilde{y}_1 \tag{A.2}$$

Changing the order of summation and integration, one gets:

$$\tilde{\hat{\mathbf{H}}}(\tilde{\mathbf{x}}', k_y, \omega) = \int_0^{L_1} \left[\sum_{n=-\infty}^{+\infty} \hat{\mathbf{H}}(\tilde{\mathbf{x}}', \tilde{y}_1 + nL_1, \omega)\exp(+\mathrm{i}k_y nL_1)\right]\exp(+\mathrm{i}k_y\tilde{y}_1)\,\mathrm{d}\tilde{y}_1 \tag{A.3}$$

Any wavenumber $k_y \in]-\infty, \infty[$ can be mapped to the wavenumber $\kappa_{y_1} \in]-\pi/L_1, \pi/L_1[$ using the relation $k_y = \kappa_{y_1} + n_1 2\pi/L_1$, where n_1 is an integer. The exponential term between square brackets in Eq. (A.3) can be expressed in terms of κ_{y_1}:

$$\tilde{\hat{\mathbf{H}}}(\tilde{\mathbf{x}}', k_y, \omega) = \int_0^{L_1} \left[\sum_{n=-\infty}^{+\infty} \hat{\mathbf{H}}(\tilde{\mathbf{x}}', \tilde{y}_1 + nL_1, \omega)\exp(+\mathrm{i}\kappa_{y_1} nL_1)\right]\exp(+\mathrm{i}k_y\tilde{y}_1)\mathrm{d}\tilde{y}_1 \tag{A.4}$$

The bracketed term is equal to the Floquet transform $\tilde{\mathbf{H}}(\tilde{\mathbf{x}}', \tilde{y}_1, \kappa_{y_1}, \omega)$. Thus, the following relation between the Floquet and the Fourier transform is obtained:

$$\tilde{\hat{\mathbf{H}}}(\tilde{\mathbf{x}}', k_y, \omega) = \int_0^{L_1} \tilde{\mathbf{H}}(\tilde{\mathbf{x}}', \tilde{y}_1, \kappa_{y_1}, \omega)\exp(+\mathrm{i}k_y\tilde{y}_1)\,\mathrm{d}\tilde{y}_1 \tag{A.5}$$

with $\kappa_{y_1} = k_y - n_1 2\pi/L_1$.

The transfer function $\tilde{\mathbf{H}}(\tilde{\mathbf{x}}', \tilde{y}, \kappa_y, \omega)$ on a larger cell of period L can be written in terms of the Fourier transform $\tilde{\hat{\mathbf{H}}}(\tilde{\mathbf{x}}', k_y, \omega)$. To derive this relation, let us start from the definition of the Floquet transform:

$$\tilde{\mathbf{H}}(\tilde{\mathbf{x}}', \tilde{y}, \kappa_y, \omega) = \sum_{n=-\infty}^{+\infty} \hat{\mathbf{H}}(\tilde{\mathbf{x}}', \tilde{y} + nL, \omega)\exp(+\mathrm{i}nL\kappa_y) \tag{A.6}$$

The function $\hat{\mathbf{H}}(\tilde{\mathbf{x}}', \tilde{y}+nL, \omega) = \hat{\mathbf{H}}(\tilde{\mathbf{x}}', y, \omega)$ can be expressed in terms of its Fourier transform $\tilde{\hat{\mathbf{H}}}(\tilde{\mathbf{x}}', k_y, \omega)$ by introducing the inverse Fourier transform:

$$\tilde{\mathbf{H}}(\tilde{\mathbf{x}}', \tilde{y}, \kappa_y, \omega) = \sum_{n=-\infty}^{+\infty} \frac{1}{2\pi} \int_{-\infty}^{\infty} \tilde{\hat{\mathbf{H}}}(\tilde{\mathbf{x}}', k_y, \omega) \exp(-\mathrm{i}k_y y)\, \mathrm{d}k_y \exp(+\mathrm{i}nL\kappa_y) \tag{A.7}$$

Changing the order of summation and integration, and introducing $y = \tilde{y} + nL$ results in to

$$\tilde{\mathbf{H}}(\tilde{\mathbf{x}}', \tilde{y}, \kappa_y, \omega) = \frac{1}{2\pi} \int_{-\infty}^{\infty} \tilde{\hat{\mathbf{H}}}(\tilde{\mathbf{x}}', k_y, \omega) \exp(-\mathrm{i}k_y \tilde{y}) \sum_{n=-\infty}^{+\infty} \exp[+\mathrm{i}nL(\kappa_y - k_y)]\, \mathrm{d}k_y \tag{A.8}$$

The identity for the Dirac comb distribution which consists of a regularly spaced infinite array of equally weighted Dirac delta functions is

$$\sum_{n=-\infty}^{\infty} \delta(y+nL) = \frac{1}{L} \sum_{m=-\infty}^{\infty} \exp\left(\mathrm{i}\frac{2\pi}{L} m y\right) \tag{A.9}$$

This identity can be used to express the summation of exponential terms in Eq. (A.8) as a summation of Dirac functions:

$$\tilde{\mathbf{H}}(\tilde{\mathbf{x}}', \tilde{y}, \kappa_y, \omega) = \frac{1}{2\pi} \int_{-\infty}^{\infty} \tilde{\hat{\mathbf{H}}}(\tilde{\mathbf{x}}', k_y, \omega) \exp(-\mathrm{i}k_y \tilde{y}) \sum_{n=-\infty}^{+\infty} \frac{2\pi}{L} \delta\left(\kappa_y - k_y + n\frac{2\pi}{L}\right) \mathrm{d}k_y \tag{A.10}$$

Integrating and simplifying one gets

$$\tilde{\mathbf{H}}(\tilde{\mathbf{x}}', \tilde{y}, \kappa_y, \omega) = \frac{1}{L} \sum_{n=-\infty}^{+\infty} \tilde{\hat{\mathbf{H}}}\left(\tilde{\mathbf{x}}', \kappa_y + n\frac{2\pi}{L}, \omega\right) \exp\left[-\mathrm{i}\left(\kappa_y + n\frac{2\pi}{L}\right)\tilde{y}\right] \tag{A.11}$$

where $\tilde{\hat{\mathbf{H}}}(\tilde{\mathbf{x}}', \kappa_y + n(2\pi/L), \omega)$ is the Fourier transform of $\hat{\mathbf{H}}(\tilde{\mathbf{x}}', y, \omega)$, but resampled according to the relation $k_y = \kappa_y + n2\pi/L$, with $k_y \in]-\infty, \infty[$ and $\kappa_y \in]-\pi/L, \pi/L[$.

Appendix B. Modelling of discontinuous floating slab tracks using a periodic approach

A semi-analytical approach for the computation of the track receptance in the case of discontinuous slabs is presented in the following. The slab discontinuity results in a periodic structure. The Floquet transform allows for the restriction of the problem domain to a generic cell $\tilde{\Omega}$. Applying the Floquet transform yields the following differential equations in the reference cell:

$$E_r I_r \frac{\mathrm{d}^4 \tilde{u}_{rz}}{\mathrm{d}\tilde{y}^4} - \omega^2 \rho_r A_r \tilde{u}_{rz} + \overline{k}_{\mathrm{rp}}(\tilde{u}_{rz} - \tilde{u}_{sz}) = \delta(\tilde{y} - \tilde{y}') \tag{B.1}$$

$$E_{\mathrm{sl}} I_{\mathrm{sl}} \frac{\mathrm{d}^4 \tilde{u}_{sz}}{\mathrm{d}\tilde{y}^4} - \omega^2 \rho_s A_s \tilde{u}_{sz} + \overline{k}_{\mathrm{sb}} \tilde{u}_{sz} - \overline{k}_{\mathrm{rp}}(\tilde{u}_{rz} - \tilde{u}_{sz}) = 0 \tag{B.2}$$

where $\tilde{u}_{rz}(\tilde{y}, \kappa_y, \omega)$ and $\tilde{u}_{sz}(\tilde{y}, \kappa_y, \omega)$ are the rail and slab displacements in the generic cell.

The following periodicity conditions of the second kind are imposed on both ends of the generic cell:

$$\frac{\mathrm{d}^m \tilde{u}_{rz}}{\mathrm{d}y^m}(L/2) = \exp(-\mathrm{i}\kappa_y L) \frac{\mathrm{d}^m \tilde{u}_{rz}}{\mathrm{d}y^m}(-L/2) \quad \text{for } m = 0, 1, 2, 3 \tag{B.3}$$

These periodic boundary conditions are imposed on the rail to allow for the wave propagation across the cells. The Neumann boundary conditions at the ends of the slab (zero shear force and bending moment) can be written as follows:

$$\frac{\mathrm{d}^m \tilde{u}_{sz}}{\mathrm{d}y^m}(-L/2) = 0 \quad \text{for } m = 2, 3 \tag{B.4}$$

$$\frac{\mathrm{d}^m \tilde{u}_{sz}}{\mathrm{d}y^m}(L/2) = 0 \quad \text{for } m = 2, 3 \tag{B.5}$$

These boundary conditions ensure that the discontinuity of the slab is accounted for in the formulation. The advantage of using the Floquet transform is that differential equations (B.1) and (B.2) have to be written only on a reference cell, which is continuous.

Eqs. (B.1) and (B.2) can be written in the following form:

$$\begin{bmatrix} E_r I_r & 0 \\ 0 & E_{\mathrm{sl}} I_{\mathrm{sl}} \end{bmatrix} \frac{\mathrm{d}^4 \tilde{\mathbf{u}}_z}{\mathrm{d}\tilde{y}^4} + \begin{bmatrix} \overline{k}_{\mathrm{rp}} - \rho_r A_r \omega^2 & -\overline{k}_{\mathrm{rp}} \\ -\overline{k}_{\mathrm{rp}} & \overline{k}_{\mathrm{rp}} + \overline{k}_{\mathrm{sb}} - \rho_{\mathrm{sl}} A_{\mathrm{sl}} \omega^2 \end{bmatrix} \tilde{\mathbf{u}}_z = \begin{bmatrix} \delta(\tilde{y} - \tilde{y}') \\ 0 \end{bmatrix} \tag{B.6}$$

where $\tilde{\mathbf{u}}_z = [\tilde{u}_{rz}, \tilde{u}_{sz}]^{\mathrm{T}}$.

The general solution of the differential equation (B.2) is the sum of the homogeneous $\tilde{\mathbf{u}}_z^h(\tilde{y},\kappa_y,\omega)$ and the particular solution $\tilde{\mathbf{u}}_z^p(\tilde{y},\kappa_y,\omega)$:

$$\tilde{\mathbf{u}}_z(\tilde{y},\kappa_y,\omega)=\tilde{\mathbf{u}}_z^h(\tilde{y},\kappa_y,\omega)+\tilde{\mathbf{u}}_z^p(\tilde{y},\kappa_y,\omega) \tag{B.7}$$

The homogeneous solution of the differential equation (B.2) can be written as follows [34,48]:

$$\tilde{\mathbf{u}}_z^h(\tilde{y},\kappa_y,\omega)=\sum_{j=1}^{8} c_j\mathbf{E}_j e^{i\alpha\tilde{y}} \tag{B.8}$$

where c_j are unknown coefficients and $\mathbf{E}_j$ are the eigenvectors of the homogeneous solution.

Since the solution sought should obey the periodicity condition of the second kind, the displacements $\tilde{\mathbf{u}}_z^p(\tilde{y},\kappa_y,\omega)$ can be expressed in terms of a function $\tilde{\boldsymbol{\phi}}(\tilde{y},\kappa_y,\omega)$ that satisfies standard periodicity conditions:

$$\tilde{\mathbf{u}}_z^p(\tilde{y},\kappa_y,\omega)=\exp(-i\kappa_y\tilde{y})\tilde{\boldsymbol{\phi}}(\tilde{y},\kappa_y,\omega) \tag{B.9}$$

where

$$\tilde{\boldsymbol{\phi}}(\tilde{y},\kappa_y,\omega)=\tilde{\boldsymbol{\phi}}(\tilde{y}+L,\kappa_y,\omega) \tag{B.10}$$

It should be noted that $\tilde{\boldsymbol{\phi}}(\tilde{y},\kappa_y,\omega)$ comprises of two periodic functions corresponding to the displacement of the rail and the slab. Since $\tilde{\boldsymbol{\phi}}(\tilde{y},\kappa_y,\omega)$ is a periodic function, it can be represented using the finite exponential Fourier series:

$$\tilde{\boldsymbol{\phi}}(\tilde{y},\kappa_y,\omega)=\sum_{n=-\infty}^{\infty}\mathbf{A}_n(\kappa_y,\omega)\exp\left(i\frac{2\pi}{L}ny\right) \tag{B.11}$$

Thus, displacements $\tilde{\mathbf{u}}_z^p(\tilde{y},\kappa_y,\omega)$ can be written as follows:

$$\tilde{\mathbf{u}}_z^p(\tilde{y},\kappa_y,\omega)=\sum_{n=-\infty}^{\infty}\mathbf{A}_n(\kappa_y,\omega)\exp\left(i\left(-\kappa_y+\frac{2\pi}{L}n\right)\tilde{y}\right) \tag{B.12}$$

Likewise, the load $\delta(\tilde{y}-\tilde{y}')$ can also be written as

$$\delta(\tilde{y}-\tilde{y}')=\frac{1}{L}\sum_{n=-\infty}^{\infty}\exp\left(i\left(-\kappa_y+\frac{2\pi}{L}n\right)(\tilde{y}-\tilde{y}')\right) \tag{B.13}$$

Eqs. (B.12) and (B.13) can be substituted in Eq. (B.6) to solve for the Fourier coefficients $\mathbf{A}_n$ of the particular solution.

The general solution $\tilde{\mathbf{u}}_z$ in the reference cell is obtained as:

$$\tilde{\mathbf{u}}_z(\tilde{y},\kappa_y,\omega)=\sum_{j=1}^{8}c_j\mathbf{E}_j e^{i\alpha\tilde{y}}+\sum_{n=-\infty}^{\infty}\mathbf{A}_n(\kappa_y,\omega)\exp\left(i\left(-\kappa_y+\frac{2\pi}{L}n\right)\tilde{y}\right) \tag{B.14}$$

The unknown coefficients c_j are determined for each frequency and wavenumber using 8 boundary conditions described by Eqs. (B.3)–(B.5). The solution $\tilde{u}_{rz}(\tilde{y},\kappa_y,\omega)$ is the track receptance $\tilde{h}_{zz}(\tilde{y}',\tilde{y},\kappa_y,\omega)$ in the frequency wavenumber domain. An inverse Floquet transformation (4) is applied to compute the track receptance $\hat{h}_{zz}(\tilde{y}',\tilde{y}+nL,\omega)$ of the discontinuous slab track in the frequency domain in the fixed frame of reference. The response of the rail $\hat{u}_r(y,\omega)$ due to a moving harmonic load $g(t)=1\exp(i\omega_m t)$ in the frequency domain can be calculated from Eq. (41). An inverse Fourier transform with respect to ω gives the displacements $u_r(y,t)$ in the time domain. The track compliance in the moving frame of reference is obtained by evaluating $u_r(y,t)$ at $y=\hat{y}_{kl}+y_{l0}+vt$, where $\hat{y}_{kl}$ is the distance between the k-th and l-th axle. These track displacements $C_{kl}^{t}(t;\omega_m)$ are periodic and can be used to calculate the periodic coefficients a_{pm}^{kl} according to Eq. (42).

References

[1] International Organization for Standardization. ISO 14837-1:2005 Mechanical vibration—Ground-borne noise and vibration arising from rail systems—Part 1: General guidance, 2005.

[2] Y.B. Yang, L.C. Hsu, A review of researches on ground-borne vibrations due to moving trains via underground tunnels, *Advances in Structural Engineering* 9 (3) (2006) 377–392.

[3] K. Abe, D. Satou, T. Suzuki, M. Furuta. Three-dimensional analysis of subway track vibrations due to running wheels. In: N. Chouw, G. Schmid (Eds.), *Proceedings of the International Workshop Wave 2000, Wave propagation, Moving load, Vibration Reduction*, Ruhr University, Germany, A.A. Balkema, Rotterdam, December 2000, pp. 149–156.

[4] L. Andersen, S.R.K. Nielsen, Reduction of ground vibration by means of barrier or soil improvement along a railway track, *Soil Dynamics and Earthquake Engineering* 25 (2005) 701–716.

[5] M. Mohammadi, D.L. Karabalis, Dynamic 3-D soil-railway track interaction by BEM–FEM, *Earthquake Engineering and Structural Dynamics* 24 (1995) 1177–1193.

[6] O. Von Estorff, M. Firuziaan, K. Friedrich, G. Pflanz, G. Schmid. A three-dimensional FEM/BEM model for the investigation of railway tracks. In: N. Chouw, G. Schmid (Eds.), *Proceedings of the International Workshop Wave 2000, Wave Propagation, Moving Load, Vibration Reduction*, Ruhr University, Germany, A.A. Balkema, Rotterdam, December 2000, pp. 157–172.

[7] C.J.C. Jones, D.J. Thompson, M. Petyt, Studies using a combined finite element and boundary element model for vibration propagation from railway tunnels. In: G. Guidati, H. Hunt, H. Heller, A. Heiss (Eds.), *7th International Congress on Sound and Vibration*, Garmisch-Partenkirchen, Germany, July 2000.

[8] O. Von Estorff, A.A. Stamos, D.E. Beskos, H. Antes, Dynamic interaction effects in underground railway traffic systems, *Earthquake Engineering and Structural Dynamics* 8 (4) (1991) 167–175.

[9] X. Sheng, C.J.C. Jones, D.J. Thompson, Prediction of ground vibration from trains using the wavenumber finite and boundary element methods, *Journal of Sound and Vibration* 293 (2006) 575–586.
[10] L. Andersen, C.J.C. Jones, Coupled boundary and finite element analysis of vibration from railway tunnels—a comparison of two- and three-dimensional models, *Journal of Sound and Vibration* 293 (2006) 611–625.
[11] X.C. Bian, E.X. Zeng, Y.M. Chen, Ground motions generated by harmonic loads moving in subway tunnel, In: Y.B. Yang, J.D. Yau (Eds.), *Proceedings of the 3rd International Symposium on Environmental Vibrations*: *Prediction*, *Monitoring*, *Mitigation and Evaluation. ISEV 2007*, Taipei, Taiwan, November 2007.
[12] Y.B. Yang, H.H. Hung, A 2.5D finite/infinite element approach for modeling visco-elastic bodies subjected to moving loads, *International Journal of Numerical Methods in Engineering* 51 (2001) 1317–1336.
[13] Y.B. Yang, H.H. Hung, Train-induced wave propagation in layered soil using finite/infinite element simulation, *Soil Dynamics and Earthquake Engineering* 23 (4) (2003) 263–278.
[14] H. Grundmann, K. Müller. Dynamic interaction of a plane elastically mounted on a tunnel. In: C. Soize (Ed.), *Proceedings of the 6th European Conference on Structural Dynamics: Eurodyn 2005*, vol. 3, Paris, France, September 2005, pp. 1273–1278.
[15] K. Müller, H. Grundmann, S. Lenz, Nonlinear interaction between a moving vehicle and a plate elastically mounted on a tunnel, *Journal of Sound and Vibration* 310 (2008) 558–586.
[16] J.A. Forrest, H.E.M. Hunt, A three-dimensional tunnel model for calculation of train-induced ground vibration, *Journal of Sound and Vibration* 294 (2006) 678–705.
[17] M.F.M. Hussein, H. Hunt, A numerical model for calculating vibration from a railway tunnel embedded in a full-space, *Journal of Sound and Vibration* 305 (2007) 401–431.
[18] M.F.M. Hussein, L. Rikse, S. Gupta, H.E.M. Hunt, G. Degrande, J.P. Talbot, S. François, M. Schevenels. Using the PiP model for fast calculation of vibration from a railway tunnel in a multi-layered half-space. In: *9th International Workshop on Railway Noise*, Munich, Germany, September 2007.
[19] D. Clouteau, M. Arnst, T.M. Al-Hussaini, G. Degrande, Freefield vibrations due to dynamic loading on a tunnel embedded in a stratified medium, *Journal of Sound and Vibration* 283 (1–2) (2005) 173–199.
[20] G. Degrande, M. Schevenels, P. Chatterjee, W. Van de Velde, P. Hölscher, V. Hopman, A. Wang, N. Dadkah, Vibrations due to a test train at variable speeds in a deep bored tunnel embedded in London clay, *Journal of Sound and Vibration* 293 (3–5) (2006) 626–644.
[21] D. Clouteau, D. Aubry, M.L. Elhabre, E. Savin, Periodic and stochastic BEM for large structures embedded in an elastic half-space, in: *Mathematical Aspects of Boundary Element Methods*, CRC Press, London, 1999, pp. 91–102.
[22] D. Clouteau, M.L. Elhabre, D. Aubry, Periodic BEM and FEM-BEM coupling: application to seismic behaviour of very long structures, *Computational Mechanics* 25 (2000) 567–577.
[23] M.L. Elhabre, Modélisation de l'interaction sismique sol-fluide-parois moulées suivant une approche périodique. Ph.D. Thesis, Laboratoire de Mécanique des Sols, Structures et Matériaux, Ecole Centrale de Paris, 2000.
[24] H. Chebli, R. Othman, D. Clouteau, Response of periodic structures due to moving loads, *Comptes Rendus Mécanique* 334 (2006) 347–352.
[25] S. Gupta, W.F. Liu, G. Degrande, G. Lombaert, W.N. Liu, Prediction of vibrations induced by underground railway traffic in Beijing, *Journal of Sound and Vibration* 310 (2008) 608–630.
[26] R.J. Craig, M. Bampton, Coupling of substructures for dynamic analyses, *AIAA Journal* 6 (7) (1968) 1313–1319.
[27] S. Gupta, M.F.M. Hussein, G. Degrande, H.E.M. Hunt, D. Clouteau, A comparison of two numerical models for the prediction of vibrations from underground railway traffic, *Soil Dynamics and Earthquake Engineering* 27 (7) (2007) 608–624.
[28] A.V. Metrikine, A.L. Bosch, Dynamic response of a two-level catenary to a moving load, *Journal of Sound and Vibration* 292 (2006) 676–693.
[29] G. Lombaert, G. Degrande, Experimental validation of a numerical prediction model for free field traffic induced vibrations by in situ experiments, *Soil Dynamics and Earthquake Engineering* 21 (6) (2001) 485–497.
[30] G. Lombaert, G. Degrande, J. Kogut, S. François, The experimental validation of a numerical model for the prediction of railway induced vibrations, *Journal of Sound and Vibration* 297 (3–5) (2006) 512–535.
[31] A. Nordborg, Wheel/rail noise generation due to nonlinear effects and parametric excitation, *Journal of the Acoustical Society of America* 111 (4) (2002).
[32] A. Nordborg. Vertical Rail Vibrations: Noise and Structure-Borne Sound Generation. Ph.D. thesis, Department of Vehicle Engineering, Royal Institute of Technology, 1995.
[33] X. Sheng, M. Li, C.J.C. Jones, D.J. Thompson, Using the Fourier-series approach to study interaction between moving wheels and periodically supported rail, *Journal of Sound and Vibration* 303 (3–5) (2007) 873–894.
[34] M.F.M. Hussein, H. Hunt, Modelling of floating-slab tracks with continuous slabs under oscillating moving loads, *Journal of Sound and Vibration* 297 (2006) 37–54.
[35] G. Lombaert, G. Degrande, B. Vanhauwere, B. Vandeborght, S. François, The control of ground borne vibrations from railway traffic by means of continuous floating slabs, *Journal of Sound and Vibration* 297 (3–5) (2006) 946–961.
[36] M.F.M. Hussein, H. Hunt, Modelling of floating-slab track with discontinuous slab. Part 1: response to oscillating moving loads, *Journal of Low Frequency Noise, Vibration and Active Control* 25 (1) (2006) 23–40.
[37] M.F.M. Hussein, H. Hunt, Modelling of floating-slab track with discontinuous slab. Part 2: response to moving trains, *Journal of Low Frequency Noise, Vibration and Active Control* 25 (2) (2006) 111–118.
[38] L. Brillouin, *Wave Propagation in Periodic Structures*, Dover Publication, 1953.
[39] S. Gupta, G. Degrande, Dynamic analysis of a beam on elastic foundation using the Fourier and Floquet transformations. Report BWM-2005-14, Department of Civil Engineering, K.U.Leuven, October 2005. SBO Project IWT 03175.
[40] X. Sheng, C.J.C. Jones, D.J. Thompson, A comparison of a theoretical model for quasi-statically and dynamically induced environmental vibration from trains with measurements, *Journal of Sound and Vibration* 267 (3) (2003) 621–635.
[41] M. Heckl, G. Hauck, R. Wettschureck, Structural-borne sound and vibration from rail traffic, *Journal of Sound and Vibration* 193 (1) (1996) 175–184.
[42] X. Sheng, C.J.C. Jones, D.J. Thompson, Prediction of ground vibration from train using the wavenumber finite and boundary element methods, *Journal of Sound and Vibration* 282 (2005) 125–149.
[43] H. Takemiya, X. Bian, Substructure simulation of inhomogeneous track and layered ground dynamic interaction under train passage, *Journal of Engineering Mechanics* 131 (2005) 699–711.
[44] A.V. Vostroukhov, A.V. Metrikine, Periodically supported beam on a visco-elastic layer as a model for dynamic analysis of a high-speed railway track, *International Journal of Solids and Structures* 40 (21) (2003) 5723–5752.
[45] L. Auersch, Ground vibration due to railway traffic—The calculation of the effects of moving static loads and their experimental verification, *Journal of Sound and Vibration* 293 (2006) 599–610.
[46] A. Hamid, T.L. Yang, Analytical description of track-geometry variations, *Transportation Research Record* 838 (1981) 19–26.
[47] P. Carels, K. Ophalffens, Floating slab track re-engineering: experience drawn from a completely renovated FST damaged by major flooding in Sao Paulo metro. In: *9th International Workshop on Railway Noise*, Munich, Germany, September 2007.
[48] M.F.M. Hussein, Vibration from underground railways. Ph.D. Thesis, Department of Engineering, University of Cambridge, 2004.